LOS ALAMOS SCIENTIFIC LABORATORY
of the
University of California
LOS ALAMOS • NEW MEXICO

Polarization Effects in Deuteron-Alpha Elastic Scattering and in the $^{3}He(d,p)^{4}He$ Reaction

UNITED STATES
ATOMIC ENERGY COMMISSION
CONTRACT W-7405-ENG. 36

This report expresses the opinions of the author or authors and does not necessarily reflect the opinions or views of the Los Alamos Scientific Laboratory.

Printed in the United States of America. Available from
Clearinghouse for Federal Scientific and Technical Information
National Bureau of Standards, U. S. Department of Commerce
Springfield, Virginia 22151
Price: Printed Copy $3.00; Microfiche $0.65

Written: February 1969
Distributed: July 1, 1969

LA-4191
UC-34, PHYSICS
TID-4500

LOS ALAMOS SCIENTIFIC LABORATORY
of the
University of California
LOS ALAMOS • NEW MEXICO

Polarization Effects in Deuteron-Alpha Elastic Scattering and in the $^{3}He(d,p)^{4}He$ Reaction*

by

Victor S. Starkovich

*This report is derived from a thesis submitted in partial fulfillment of the requirements for the degree of Doctor of Philosophy in physics from the Graduate School of the University of Wyoming.

ACKNOWLEDGEMENTS

I am deeply grateful to Dr. Gerald G. Ohlsen, Dr. William G. Simon, and Dr. Eugene M. Bernstein under whose co-direction this investigation was conducted. Particular thanks are due Dr. Ohlsen for his helpful assistance and guidance during the course of this work. I am grateful also to Dr. D. C. Dodder and Dr. P. W. Keaton for many helpful discussions.

I would like to thank Mrs. Marjorie Peacock and Mrs. Kathleen Witte for assistance in the use of computer programs, and Dr. L. C. McIntyre and Dr. W. Haeberli for providing a spin-one phase-shift code.

For financial assistance gratitude is extended to the U. S. Atomic Energy Commission and the Associated Western Universities.

TABLE OF CONTENTS

CHAPTER

LIST OF TABLES

LIST OF FIGURES

FIGURE Page

ABSTRACT

POLARIZATION EFFECTS IN DEUTERON-ALPHA ELASTIC SCATTERING AND IN THE $^{3}He(d,p)^{4}He$ REACTION

Victor S. Starkovich

Azimuthal asymmetries produced in deuteron-alpha double scattering have been measured for a range of second-scattering angles. It has been demonstrated that d-α elastic scattering can be used to produce a deuteron beam with useful vector polarization at energies near 10 MeV. It has also been shown that d-α scattering can provide a useful absolute calibration for the vector polarization of a beam of deuterons produced by a polarized-ion source.

Left-Right proton asymmetries for the $^{3}He(d,p)^{4}He$ reaction have been measured using a polarized deuteron beam obtained from d-α elastic scattering. Measurements were made for deuteron energies of 10.0, 12.0, and 14.0 MeV, extending the range of similar measurements made at the University of Wisconsin.

CHAPTER I

INTRODUCTION

In an effort to better understand the nature of nuclear forces, an ever increasing number of experiments involving polarized nuclei are being conducted. Such experiments supplement differential cross section measurements and help to provide information on the spin dependence of the nuclear interaction.

The first nucleon polarization experiment was conducted by Heusinkveld *et al.* in 1952 (He 52). Since that time the majority of polarization experiments have involved nucleons, and relatively few measurements have been done involving spin-one particles such as deuterons. In the study of deuteron interactions with nuclei, polarization measurements are particularly useful, since the spin dependence of the interaction is considerably more complex for spin-one particles than for the case of particles of spin-1/2.

The first deuteron polarization experiment was conducted by Chamberlain in 1954 (Ch 54), and involved scattering deuterons twice from carbon at a deuteron energy of 167 MeV. Since that time, additional high-energy deuteron double-scattering experiments have been performed by Baldwin *et al.* (Ba 56) in the 94-157 MeV energy range, and by Button *et al.* (Bu 60) at 420-MeV deuteron energy. Double-scattering experiments have also been conducted near 6-MeV deuteron energy (Al 60, Ne 64).

In addition to double-scattering experiments, deuteron polarization measurements at low energies have employed reactions with known analyzing powers (Po 61, Se 64a, Mc 65, Yo 65, Br 66, Yo 67). Experiments to determine polarization parameters have also been conducted using polarized-ion sources in conjunction with tandem accelerators and cyclotrons (Be 63, Ar 65, Ar 67, Ex 67, Sc 68).

The experiments to be described in this thesis were undertaken in order to provide information useful in the description of the five and six nucleon systems. In addition, measurements are presented which can serve as a standard in the absolute calibration of polarized-ion sources. Only a brief discussion of the material is included here.

Chapter II and the Appendix contain a brief description of a mathematical formalism which is useful in the characterization of a polarized beam of spin-one particles. The spin tensor moments $\langle iT_{11} \rangle$, $\langle T_{20} \rangle$, $\langle T_{21} \rangle$, and $\langle T_{22} \rangle$ are described in terms of the density matrix and, for visualization purposes, an analogy is made between these tensors and the multipole moments of a static charge distribution. The Appendix describes the rotation properties of these spin tensor moments.

In Chapters III and IV, the results of a study of d-^{4}He elastic scattering are presented. Azimuthal asymmetries produced in d-^{4}He double scattering at 9.0-MeV equivalent deuteron energy (both scatterings) are presented in Chapter III, along with the results of a phase-shift analysis using these measurements in conjunction with previously existing d-^{4}He cross section data. The measured asymmetries

are in excellent agreement with those subsequently taken at the University of Wisconsin (Lo 67). Phase-shift predictions based on these measurements are consistent with the phase predictions of Trier et al. (Tr 67), conducted at lower deuteron energies.

In Chapter IV, data obtained from d-^{4}He double scattering at 11.5-MeV deuteron energy (both scatterings), and over a range of second-scattering angles which includes the first-scattering angle, are presented. It is shown how this information may be used to provide an absolute calibration for the polarization of a beam of deuterons produced by a polarized-ion source. Phase-shift solutions involving these measurements are consistent with those obtained at 9.0-MeV deuteron energy.

An investigation of the ^{3}He(d,p)^{4}He reaction with a polarized deuteron beam obtained from d-^{4}He elastic scattering is discussed in Chapter V. Right-to-Left proton asymmetry measurements were made for deuteron energies of 10.0, 12.0, and 14.0 MeV. The largest value of R/L ($\sim$3.47$\pm$0.27) occurred at 121° (c.m.) for 10.0-MeV incident deuterons.

CHAPTER II

DESCRIPTION OF THE SPIN POLARIZATION OF THE DEUTERON

2.1 Introduction

In preparation for the study of deuteron-alpha elastic scattering, it was necessary to review the theoretical description of the scattering and polarization of spin-one particles. This chapter, in conjunction with the Appendix, contains a summary of some of the methods and parameters used in such a description. Detailed treatments of the subject have been given by W. Lakin (La 55), G. R. Satchler (Sa 60), and U. Fano (Fa 57).

The description of the polarization of spin-one particles is considerably more complex than the description for particles of spin-1/2. In the latter case, the degree of polarization (P) of a nucleon beam with respect to a particular axis of quantization can be written

$$P = \frac{N_{\uparrow} - N_{\downarrow}}{N_{\uparrow} + N_{\downarrow}} ,$$

where $N_{\uparrow}$ and $N_{\downarrow}$ represent the relative numbers of particles in the two possible spin states (spin up and spin down).

No such simple description exists for the case of spin-one particles. For the spin-one system there exist three possible magnetic substates, in one of which the component of the spin along the axis of quantization vanishes ($m_I=0$). Since the spin-one system

is not, in general, symmetric about any single axis, the polarization cannot be completely described in a simple manner in terms of the relative numbers of particles $N_{\uparrow}$, N_o, and $N_{\downarrow}$ in the three eigenstates. However, the polarization of such a system can be conveniently described by certain spin tensor operators T_{KQ}, which will be discussed in terms of the density matrix in the following section. The expectation values of the operators T_{KQ} will henceforth be referred to as spin tensor moments. An outline of the density matrix formalism will be followed by an explanation of the use of the spin tensor moments, and an analogy between the spin moments and the multipole moments of a static charge distribution.

2.2 Density Matrix Description of Deuteron Polarization

Although the von Neumann Density Matrix ρ was introduced in 1927 (Ne 27), it was not until 1952 that Wolfenstein and Ashkin (Wo 52) and, independently, Dalitz (Da 52) used the density matrix formalism as a starting point in discussing polarization phenomena. The density matrix offers an elegant and useful way of describing polarized beams of particles, since such beams are statistical mixtures of a number of pure spin states.

For the spin-one system, the spin-wave function χ can be characterized by the spinor $\chi=\begin{bmatrix} C_1 \\ C_2 \\ C_3 \end{bmatrix}$ where the quantities $|C_1|^2$, $|C_2|^2$, and $|C_3|^2$ represent the probability of finding the system in each of its three respective spin states (m_I=1, 0, -1) and where

$$|C_1|^2 + |C_2|^2 + |C_3|^2 = 1.$$

According to the probability doctrine of quantum mechanics, knowledge of the density matrix completely determines the state of the system. For example, the expectation value of an arbitrary operator O can be determined by writing (Me 61):

$$\langle O \rangle = \chi^* O \chi$$

$$= [C_1^* \; C_2^* \; C_3^*] \begin{bmatrix} O_{11} & O_{12} & O_{13} \\ O_{21} & O_{22} & O_{23} \\ O_{31} & O_{32} & O_{33} \end{bmatrix} \begin{bmatrix} C_1 \\ C_2 \\ C_3 \end{bmatrix}$$

$$\langle O \rangle = |C_1|^2 O_{11} + C_1 C_2^* O_{21} + C_1 C_3^* O_{31}$$

$$+ C_2 C_1^* O_{12} + |C_2|^2 O_{22} + C_2 C_3^* O_{32}$$

$$+ C_3 C_1^* O_{13} + C_3 C_2^* O_{23} + |C_3|^2 O_{33}$$

or, rewriting:

$$\langle O \rangle = \text{trace} \begin{bmatrix} |C_1|^2 & C_2 C_1^* & C_3 C_1^* \\ C_1 C_2^* & |C_2|^2 & C_3 C_2^* \\ C_1 C_3^* & C_2 C_3^* & |C_3|^2 \end{bmatrix} \begin{bmatrix} O_{11} & O_{12} & O_{13} \\ O_{21} & O_{22} & O_{23} \\ O_{31} & O_{32} & O_{33} \end{bmatrix} .$$

Hence, we have the fundamental formula: $\langle O \rangle = \text{Tr}(\rho O)$, where ρ is the density matrix. The density matrix is hermitean, positive definite and of unit trace.

The density matrix formalism can also be made to apply to an ensemble of particles by introducing a summation over the total number

of particles N in the ensemble. In such a case the quantity $|C_1|^2$ would, for example, be replaced by the summation $\sum_{n=1}^{N} |C_1^n|^2$.

Accordingly, the polarization state of a system of particles with spin S can be specified by a 2S+1 by 2S+1 dimensional hermitean matrix with unit trace, involving $(2S+1)^2-1$ complex parameters.

If the density matrix is expanded in terms of a complete set of orthogonal operators, the coefficients in this expansion completely determine the density matrix and, therefore, may be used as parameters to specify the polarization state of the system. The spin tensor moments $\langle T_{KQ} \rangle$ are coefficients of this type. A set of $(2S+1)^2$ operators T_{KQ} are chosen with the orthogonality condition

$$\mathrm{Tr}(T_{KQ}\, T_{KQ}^{\dagger}) = (2S+1)\, \delta_{KK'}\, \delta_{QQ'},$$

($\dagger$ indicates the hermitean conjugate), and the density matrix expanded as

$$\rho = \frac{1}{2S+1} \sum_{KQ} \langle T_{KQ} \rangle\, T_{KQ}^{\dagger},$$

where K is the rank of the tensor and $|Q| \leq K \leq 2S$. In the case of a spin-one system, nine orthogonal operators must be chosen to serve as a basis for the expansion of the density matrix (Si 53). The density matrix then becomes (Sc 67):

$$\rho=\frac{1}{3}\begin{bmatrix} 1+\sqrt{\frac{3}{2}}\langle T_{10}\rangle+\sqrt{\frac{1}{2}}\langle T_{20}\rangle & \sqrt{\frac{3}{2}}(\langle T_{1-1}\rangle+\langle T_{2-1}\rangle) & \sqrt{3}\langle T_{2-2}\rangle \\ -\sqrt{\frac{3}{2}}(\langle T_{11}\rangle+\langle T_{21}\rangle) & 1-\sqrt{2}\langle T_{20}\rangle & \sqrt{\frac{3}{2}}(\langle T_{1-1}\rangle-\langle T_{2-1}\rangle) \\ \sqrt{3}\langle T_{22}\rangle & -\sqrt{\frac{3}{2}}(\langle T_{11}\rangle-\langle T_{21}\rangle) & 1-\sqrt{\frac{3}{2}}\langle T_{10}\rangle+\sqrt{\frac{1}{2}}\langle T_{20}\rangle \end{bmatrix} .$$

2.3 The Spin Tensor Moments

The expectation values of the operators T_{KQ} used in this experiment can be written in terms of the components of the spin-one operator $\vec{S}$ (La 55):

$$\begin{aligned} \langle T_{00}\rangle &= 1 & \langle T_{10}\rangle &= \sqrt{\tfrac{3}{2}}\,\langle S_Z\rangle \\ \langle T_{1\pm1}\rangle &= \mp\sqrt{\tfrac{3}{2}}\,\langle S_X \pm iS_Y\rangle \\ \langle T_{20}\rangle &= \sqrt{\tfrac{1}{2}}\,\langle 3S_Z^2 - 2\rangle \\ \langle T_{2\pm1}\rangle &= \mp\sqrt{\tfrac{3}{2}}\,\langle (S_X \pm iS_Y)S_Z + S_Z(S_X \pm iS_Y)\rangle \\ \langle T_{2\pm2}\rangle &= \sqrt{\tfrac{3}{2}}\,\langle (S_X \pm iS_Y)^2\rangle \ , \end{aligned} \qquad (2.1)$$

where

$$S_X = \sqrt{\tfrac{1}{2}}\begin{bmatrix} 0 & 1 & 0 \\ 1 & 0 & 1 \\ 0 & 1 & 0 \end{bmatrix} \quad , \quad S_Y = \sqrt{\tfrac{1}{2}}\begin{bmatrix} 0 & -i & 0 \\ i & 0 & -i \\ 0 & i & 0 \end{bmatrix} \ ,$$

$$S_Z = \begin{bmatrix} 1 & 0 & 0 \\ 0 & 0 & 0 \\ 0 & 0 & -1 \end{bmatrix} \ ,$$

(Sc 55, Eq. 24.15).

A system of particles for which some of the $\langle T_{1Q} \rangle$ are non-zero is referred to as being vector polarized. Tensor, or second-rank polarization is said to exist when some of the $\langle T_{2Q} \rangle$ are non-vanishing. The moment $\langle T_{00} \rangle$ is related to the beam intensity and does not contain any information on the spin states involved.

Although other parameters have been used to describe spin-one polarization, these tensor moments possess a distinct advantage because of their spatial rotation properties (see Appendix). In addition, this representation is especially convenient in the case of spin-one particles since the tensors relate to the differential cross section in an uncomplicated manner.

On the basis of invariance properties resulting from parity considerations, certain conditions are imposed on the spin tensor moments $\langle T_{KQ} \rangle$, depending upon the choice of quantization axis (Ja 59, Ra 64, Sh 57). In particular, if a right-handed coordinate system is chosen in which the z-axis is along the wave vector of the outgoing particle and the y-axis is along the normal to the scattering plane (the usual choice of quantization axis), the moments 2.1 are subject to the following restrictions:

1. $\langle T_{KO} \rangle = 0$ if K is odd;
2. $\langle T_{KQ} \rangle$ is real if K is even;
3. $\langle T_{KQ} \rangle$ is imaginary if K is odd.

If these general rules, as well as the conjugation property $\langle T_{KQ} \rangle = (-1)^{Q} \langle T_{K\bar{Q}} \rangle^{*}$ are applied, only four real parameters are

---

*Denotes complex conjugate,

necessary to completely describe the spin-one system. The four parameters in terms of the components of the spin-one operators are:

$$\langle iT_{11}\rangle = \frac{\sqrt{3}}{2}\langle S_Y\rangle, \quad \langle T_{20}\rangle = \sqrt{\frac{1}{2}}\langle 3S_Z^2 - 2\rangle ,$$

$$\langle T_{21}\rangle = \frac{-\sqrt{3}}{2}\langle iS_YS_Z + iS_ZS_Y\rangle , \tag{2.2}$$

$$\langle T_{22}\rangle = \frac{-\sqrt{3}}{2}\langle S_Y^2\rangle .$$

The theoretical limits on these quantities are:

$$\frac{-\sqrt{3}}{2} \le \langle iT_{11}\rangle \le \frac{\sqrt{3}}{2} \qquad -\sqrt{2} \le \langle T_{20}\rangle \le \frac{\sqrt{2}}{2}$$

$$\tag{2.3}$$

$$\frac{-\sqrt{3}}{2} \le \langle T_{21}\rangle \le \frac{\sqrt{3}}{2} \qquad \frac{-\sqrt{3}}{2} \le \langle T_{22}\rangle \le \frac{\sqrt{3}}{2} .$$

All of the above quantities are functions of the deuteron energy and the angle of scattering. The vector polarization $\langle iT_{11}\rangle$ is proportional to the expectation value of the y component of the spin operator, and is perpendicular to the scattering plane. The three tensor polarization parameters are not as easily visualized since they involve quadratic combinations of the components of the spin operator. As an aid in picturing these parameters, an analogy between them and the multipole moments of a static charge distribution will be presented in the following section.

2.4 The Spin Tensor Moments and Their Analogous Electric Charge Distribution

A spin system can be completely specified by its spin moments in much the same way that an electric charge distribution is completely specified by giving its complete set of multipole moments (Da 67, Bl 59). Thus, the vector polarization components $\langle T_{1Q} \rangle$ would be analogous to the components of the dipole moment, while the $\langle T_{2Q} \rangle$ would have as their counterpart the quadrupole moments of the charge distribution. The monopole moment would be analogous to the intensity of the beam.

The ellipsoids illustrating separately all three of the second-rank polarizations are shown in Figs. 1-3. A tensor polarized beam characterized by a non-vanishing $\langle T_{20} \rangle$ is shown in Fig. 1. The ellipsoid is symmetric about the beam axis, and, thus, the moment $\langle T_{20} \rangle$ may be thought of as a measure of the average spin projection on the z-axis. If such a tensor-polarized beam initiates a reaction or is scattered, the outgoing particle intensity would be independent of azimuthal angle. Figure 2 represents a particle beam for which only $\langle T_{21} \rangle$ is non-zero. If the ellipsoid is viewed from above, it can be seen that this tensor component will produce a left-right asymmetry in the intensity of the outgoing particles. As in the case of a vector polarized beam, this asymmetry is expressed by a $\cos \phi$ factor, where ϕ is the azimuthal angle. Finally, if the particle beam contains only $\langle T_{22} \rangle$ polarization, as shown in Fig. 3, a difference between the intensities of the particles emitted vertically and horizontally will

result. Since the intensity variation is periodic ($I(\phi)=I(\phi+\pi)$), the parameter $\langle T_{22} \rangle$ would be expected to have a $\cos 2\phi$ azimuthal dependence. Thus, the analogy is useful in obtaining a qualitative idea of the effects introduced by the second-rank moments. The azimuthal dependence of these moments is illustrated again in Eq. (3.1), which is the cross section expression for the second scattering of a polarized deuteron beam.

Figures 1-3. Ellipsoids illustrating separately all three of the second-rank polarizations. Figure 1 represents the moment $\langle T_{20} \rangle$, which is symmetric about the beam axis (z-axis). Figure 2 illustrates a particle beam for which only $\langle T_{21} \rangle$ is non-zero. Figure 3 characterizes a particle beam which contains only $\langle T_{22} \rangle$ polarization. The beam axis in every case corresponds to the z-axis.

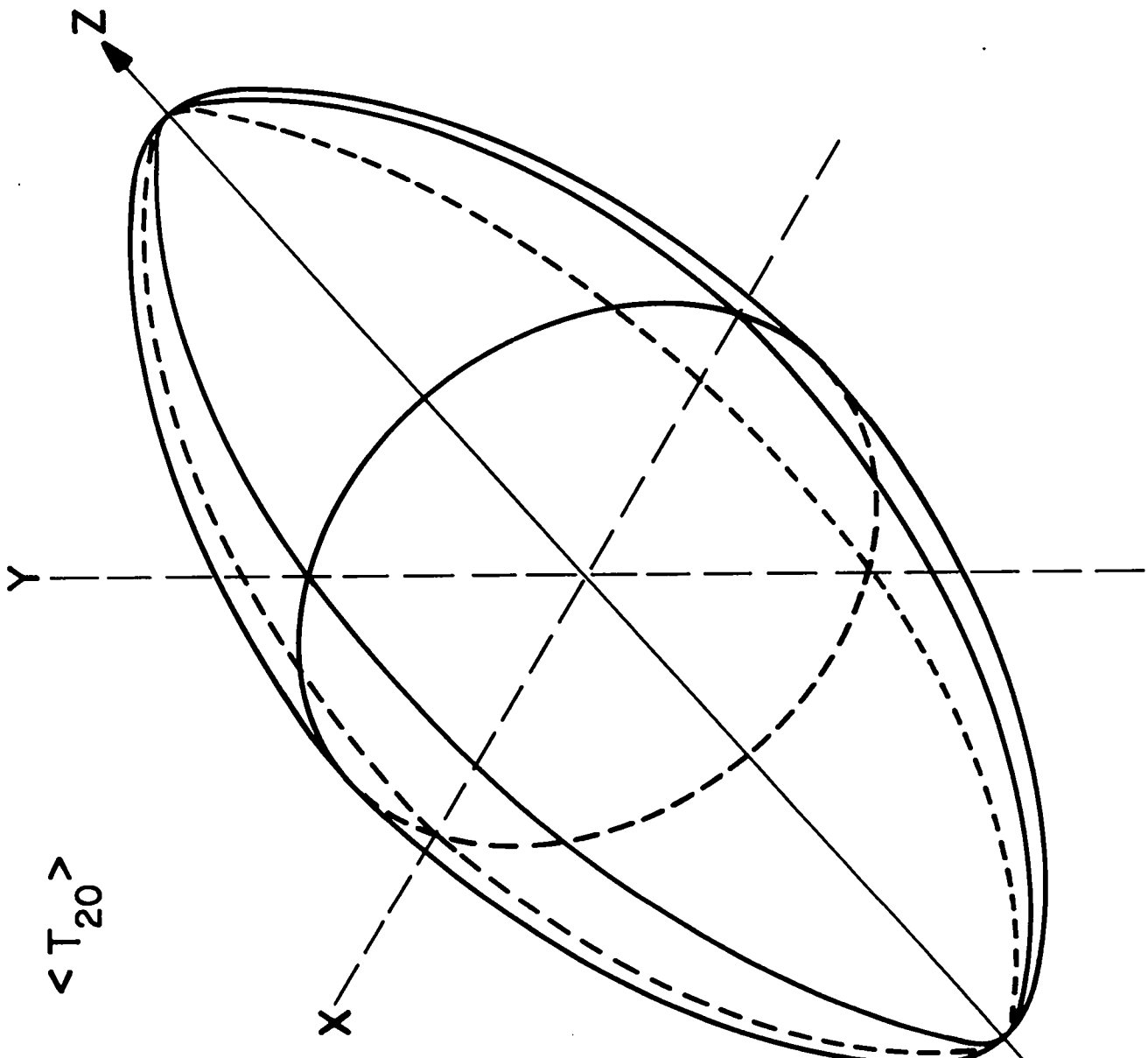

Fig. 1

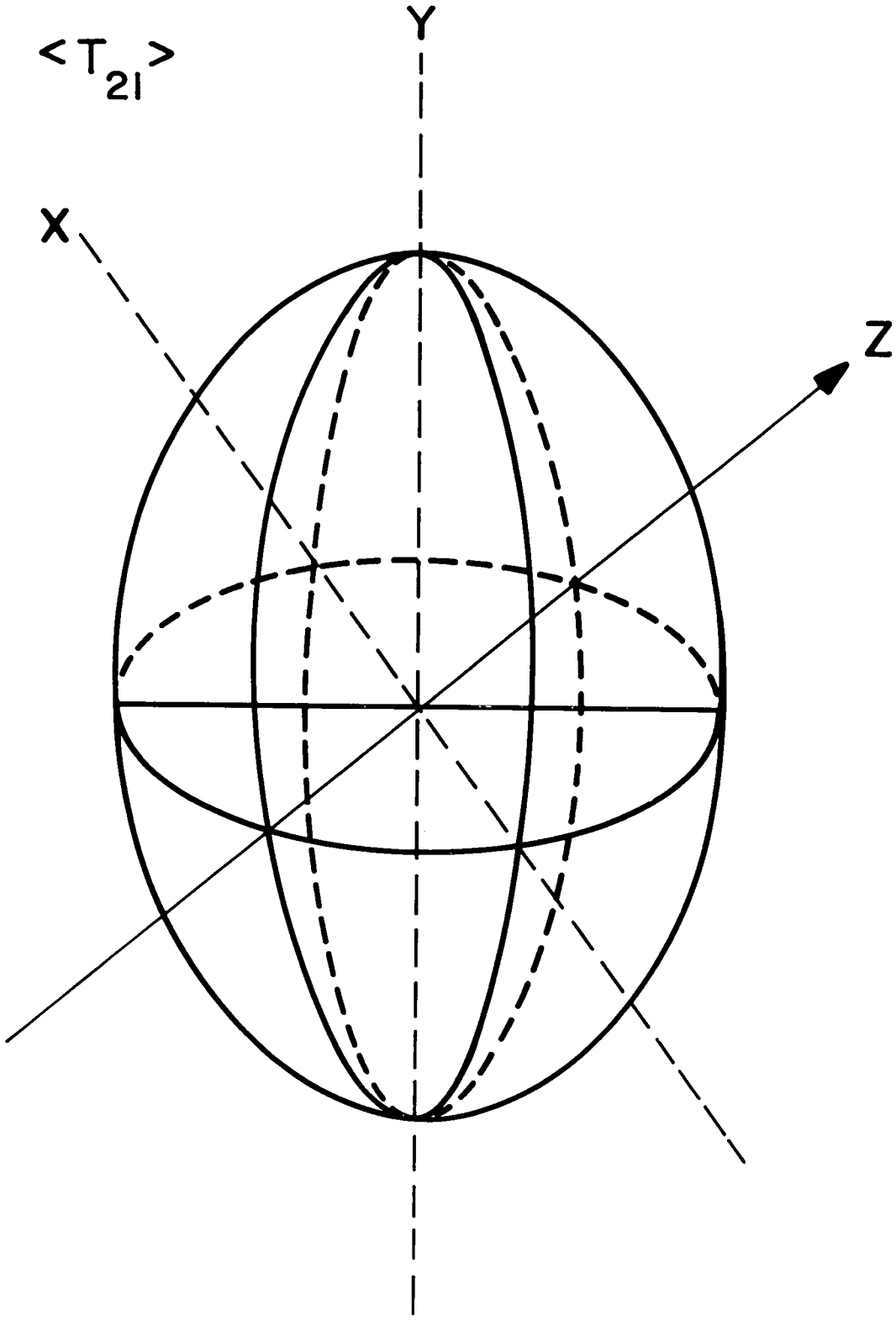

Fig. 2

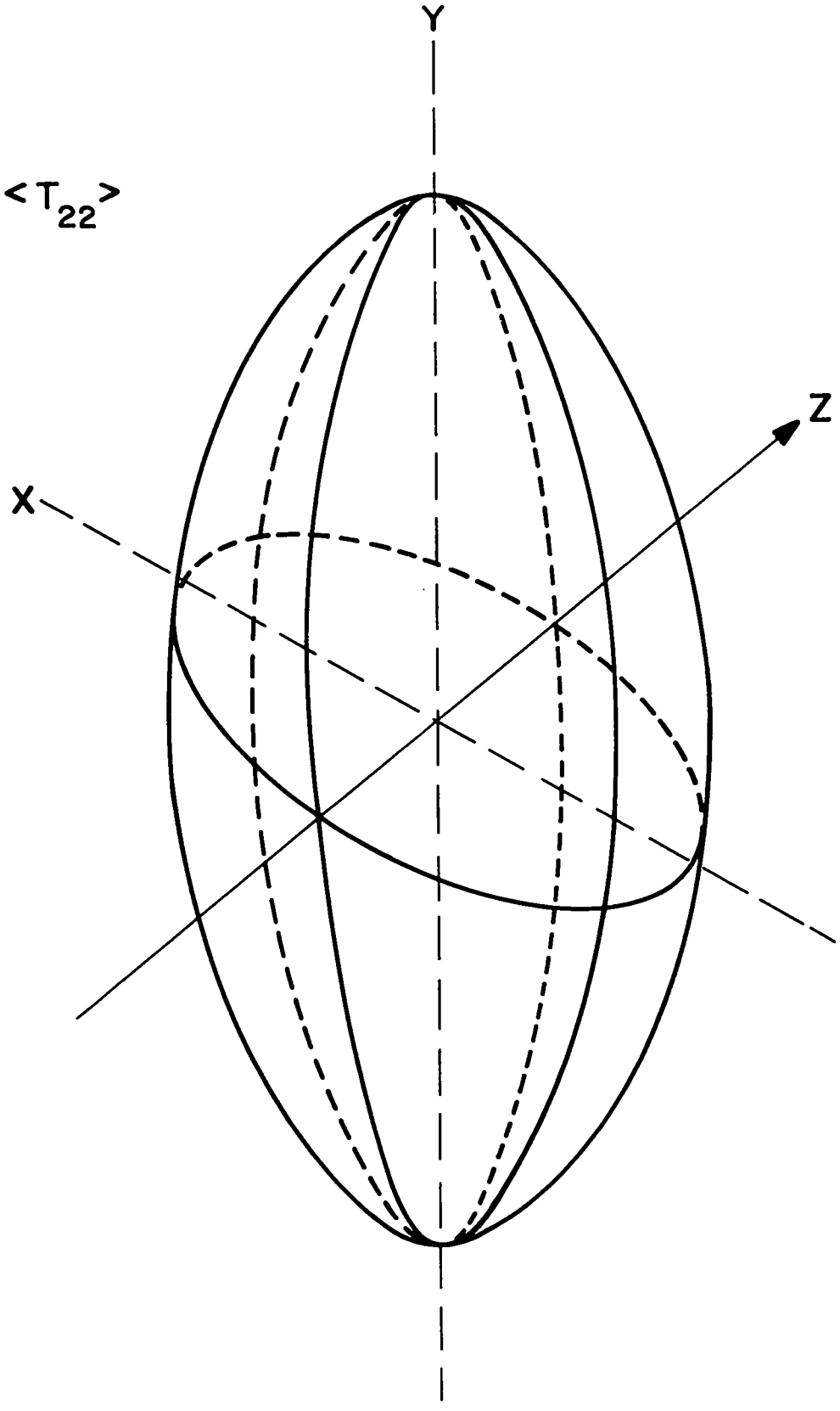

Fig. 3

CHAPTER III

DEUTERON POLARIZATION FROM DEUTERON-ALPHA ELASTIC SCATTERING

3.1 Introduction

Both in its experimental and theoretical features, the double scattering of deuterons is more complicated than nucleon-nucleus double scattering. For a given incident polarization the second-scattered intensity of nucleons may be described by but one parameter in addition to the unpolarized cross section--namely, the polarization. For deuterons, however, because they have spin-one, four parameters in addition to the unpolarized cross section may in principle be measured. Because of the more complex formalism needed to describe deuteron elastic scattering, the results of deuteron polarization experiments are needed for a better understanding of the nature of the deuteron-nucleus interaction.

The experiments to be described in the following two chapters involve the determination of the spin orientation of initially unpolarized deuterons that have been elastically scattered by ^{4}He. The results of this investigation were used in three different ways. As will be discussed in Chapter IV, it has been demonstrated that d-^{4}He elastic scattering can provide an absolute calibration for the vector polarization of a beam of deuterons produced by a polarized-ion source. Secondly, these measurements have demonstrated that a useful vector-polarized deuteron beam can be obtained from deuteron-

alpha elastic scattering at energies near 10 MeV. Thirdly, when employed in a phase-shift analysis, in conjunction with the tensor polarization parameters and differential cross section, the vector polarization provides additional constraints on the phase shifts, and hence aids in resolving the ambiguities which usually arise when cross sections alone are available.

The differential cross sections for the second scattering in a double-scattering experiment may be written as follows (La 55*, St 55, Bu 60, Sa 60**):

$$\sigma(\theta_2,\phi_2) = \sigma_o(\theta_2)[a(\theta_2)+b(\theta_2)\cos\phi_2+c(\theta_2)\cos 2\phi_2] \qquad (3.1)$$

where

$$a(\theta_2) = 1 + \langle T_{20}\rangle_1\langle T_{20}\rangle_2$$

$$b(\theta_2) = 2(\langle iT_{11}\rangle_1\langle iT_{11}\rangle_2 - \langle T_{21}\rangle_1\langle T_{21}\rangle_2)$$

$$c(\theta_2) = 2\langle T_{22}\rangle_1\langle T_{22}\rangle_2 \ .$$

The unpolarized cross section is $\sigma_o(\theta_2)$ where θ_2 is the center-of-mass angle for the second scattering. The properties of the parameters $\langle T_{KQ}\rangle$ are discussed in Chapter II and the Appendix. The tensors with subscript 1 characterize the once-scattered beam and are referred to the incident laboratory direction for the second scattering (as the z-axis). The tensors with subscript 2 are the polarization values

*The sign of the term containing $\langle T_{21}\rangle$ is in error in these references.

**Satchler uses tensor moments with the y-axis in the direction $\vec{k}_{out}\times\vec{k}_{in}$.

which would have been produced by an unpolarized beam and are referred to the outgoing center-of-mass direction (as the z-axis). The y-axis for both sets of parameters is in the direction $\vec{k}_{in} \times \vec{k}_{out}$.

The following investigation determines the azimuthal asymmetries 1) (Right to Left) and 2) (Up plus Down) to (Right plus Left) produced in d-^{4}He elastic scattering at 9.0-, and 11.0-MeV deuteron energies. Both first scatterings take place at the same center-of-mass energy, which corresponds to 9.0-MeV deuterons. Information obtained from the present experiment in conjunction with previously existing results, is sufficient to determine the deuteron vector polarization $\langle iT_{11} \rangle_2$ for d-^{4}He double scattering.

3.2 Apparatus

3.2a The Experimental Beam Tube

The basic experimental apparatus is shown in Fig. 4. The system consisted of a liquid-nitrogen-cooled deuterium target, quadrupole focusing lens, absorber foils, ^{4}He gas-filled chamber, and four E-ΔE detector telescopes. The first gas target contained deuterium and was bombarded with alpha particles from the Los Alamos Variable Energy Cyclotron (LAVEC). The recoiling deuterons were then passed through the quadrupole focusing lens, slowed with absorber foils (so that both scatterings occurred at the same center-of-mass energy) and allowed to enter the ^{4}He gas-filled chamber. Scattered deuterons were then detected with four pairs of E-ΔE semiconductor detectors set at a given θ_2 and azimuthal angles ϕ_2=0, 90, 180, and 270 degrees. The detector telescopes, which were mounted inside the scattering

Figure 4. Cross-sectional view of the double-scattering apparatus used in the deuteron-alpha polarization measurements. Also indicated is an end view of the ^{4}He gas-filled target chamber. (The figure is not drawn to scale.)

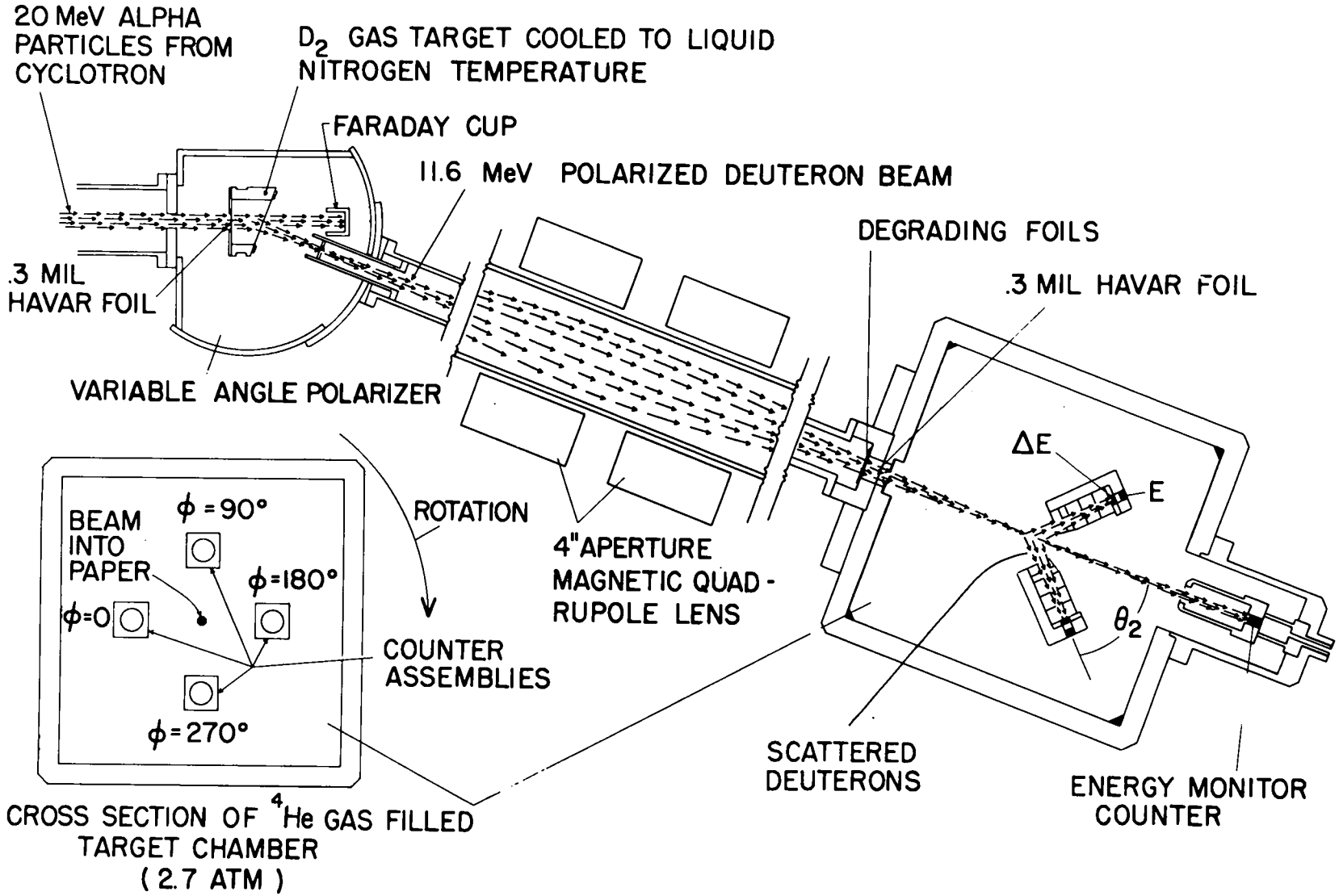
20 MeV ALPHA PARTICLES FROM CYCLOTRON
D_2 GAS TARGET COOLED TO LIQUID NITROGEN TEMPERATURE
FARADAY CUP
11.6 MeV POLARIZED DEUTERON BEAM
DEGRADING FOILS
.3 MIL HAVAR FOIL
.3 MIL HAVAR FOIL
VARIABLE ANGLE POLARIZER
ROTATION
4" APERTURE MAGNETIC QUADRUPOLE LENS
ΔE
E
θ_2
BEAM INTO PAPER
$\phi = 90°$
$\phi = 180°$
$\phi = 0$
$\phi = 270°$
COUNTER ASSEMBLIES
SCATTERED DEUTERONS
ENERGY MONITOR COUNTER
CROSS SECTION OF ^4He GAS FILLED TARGET CHAMBER (2.7 ATM)

Fig. 4

chamber, could be positioned at a given angle θ_2 by means of external circular verniers. The telescopes could easily be removed, interchanged, or positioned radially with respect to the polarized beam.

Aluminum absorber foils (to slow the scattered deuterons) were placed well in front of the collimator to the second-scattering chamber. This placement essentially eliminated the effects of foil-scattered particles.

The rear of the second-scattering chamber contained a mount for an energy-monitor detector. This semiconductor detector was positioned such that it could measure the entire energy spectrum of the deuterons as they entered the scattering chamber under normal running conditions.

A computer program called TRANSPORT* was employed to improve the design of the secondary beam transport system. It was used to determine the optimum slit sizes, beam-tube diameter and length, and quadrupole focusing current for the various experiments.

The first scattering chamber and quadrupole lens system have been previously used in the proton double-scattering experiments of Rosen et al. (Ro 65). The second-scattering chamber, slits, beam tube, and gas-handling systems are peculiar to this experiment.

3.2b The Second-Scattering Chamber

The second-scattering chamber shown in Fig. 4 is cubic in shape with inside dimensions of 12-1/2 inches on a side. Independently

*Written by C. H. Moore, S. K. Howry, and A. S. Butler, Stanford University.

rotatable detector-slit systems were mounted from the four sides of the chamber and were used simultaneously for the measurements. The detector systems rotated on bushings, and the vacuum seals were accomplished with "O"-rings positioned within the walls of the chamber. The angles of the detectors could be set to an accuracy of ±0.1 degrees by means of circular verniers on the outer surfaces of the scattering chamber. All important dimensions of the chamber were specified to be held within ±0.002 inch of their stated values.

In order to cancel small differences in counter efficiencies, solid angles, and scattering angles, the second-scattering chamber was designed to rotate about the beam axis. By employing a Havar* foil and a specially designed rotating seal, it was possible to maintain the vacuum in the beam tube and the gas pressure in the scattering chamber while rotating the chamber about the beam axis. The azimuthal position of the detectors was determined by an additional circular vernier located at the rear of the scattering chamber. Coaxial vacuum feedthroughs in the walls of the chamber were used to connect the external detector signal and bias lines to the E and ΔE detectors within the chamber.

The scattering chamber was designed in such a fashion that the energy monitor-detector system could be interchanged with special devices for positioning nuclear emulsions, gold foils, and a ^{3}He gas cell at the center of the chamber. This design proved useful in

---

*A high tensile strength cobalt alloy obtained from the Precision Metals Division of the Hamilton Watch Company.

the alignment procedure and simplified the later study of the $^{3}He(d,p)^{4}He$ reaction.

3.2c Detector Slit Assemblies

The essential features of the detector slit systems used in this experiment are shown in Fig. 5. Particles scattered into each detector system were collimated by a rectangular slit arrangement which consisted of four anti-scattering slits placed between a front and rear slit. Ortec silicon transmission detectors (ΔE), which were about 50 microns in thickness were placed immediately behind the rear slit in each system and were used to determine the rate of energy loss of the incoming particles. Surface barrier detectors to determine the energy of the particles (E) were placed immediately behind the ΔE counters and were of sufficient thickness (500 microns) to stop the elastically-scattered deuterons.

As mentioned previously, the detectors and their slit assemblies could be positioned radially with respect to the beam. However, because of their physical size, all four telescopes could only be used over the 30°-150° angular range (lab). Consequently, only Right-to-Left asymmetry measurements were obtained at angles smaller than 30° (lab).

With 2.7 atmospheres (absolute) of ^{4}He in the second-scattering chamber, distances and ΔE counter thicknesses were sufficiently large to prevent deuterons of 3 MeV or less (resulting from the second scattering) from reaching the E detectors. Consequently, the asymmetry measurements were limited to angles smaller than 130° (c.m.).

Figure 5. Cross-sectional view of the detector slit assemblies employed in the deuteron polarization measurements. The detector slits were constructed of brass.

Front Slit Width = 0.350 in.

Rear Slit Width = 0.350 in.

Front and Rear Slit Thickness = 0.062 in.

Antiscatter slit thickness = 0.020 in.

h = 2.50 in.

R_o = 3.50 in.

DETECTOR SLIT ASSEMBLY

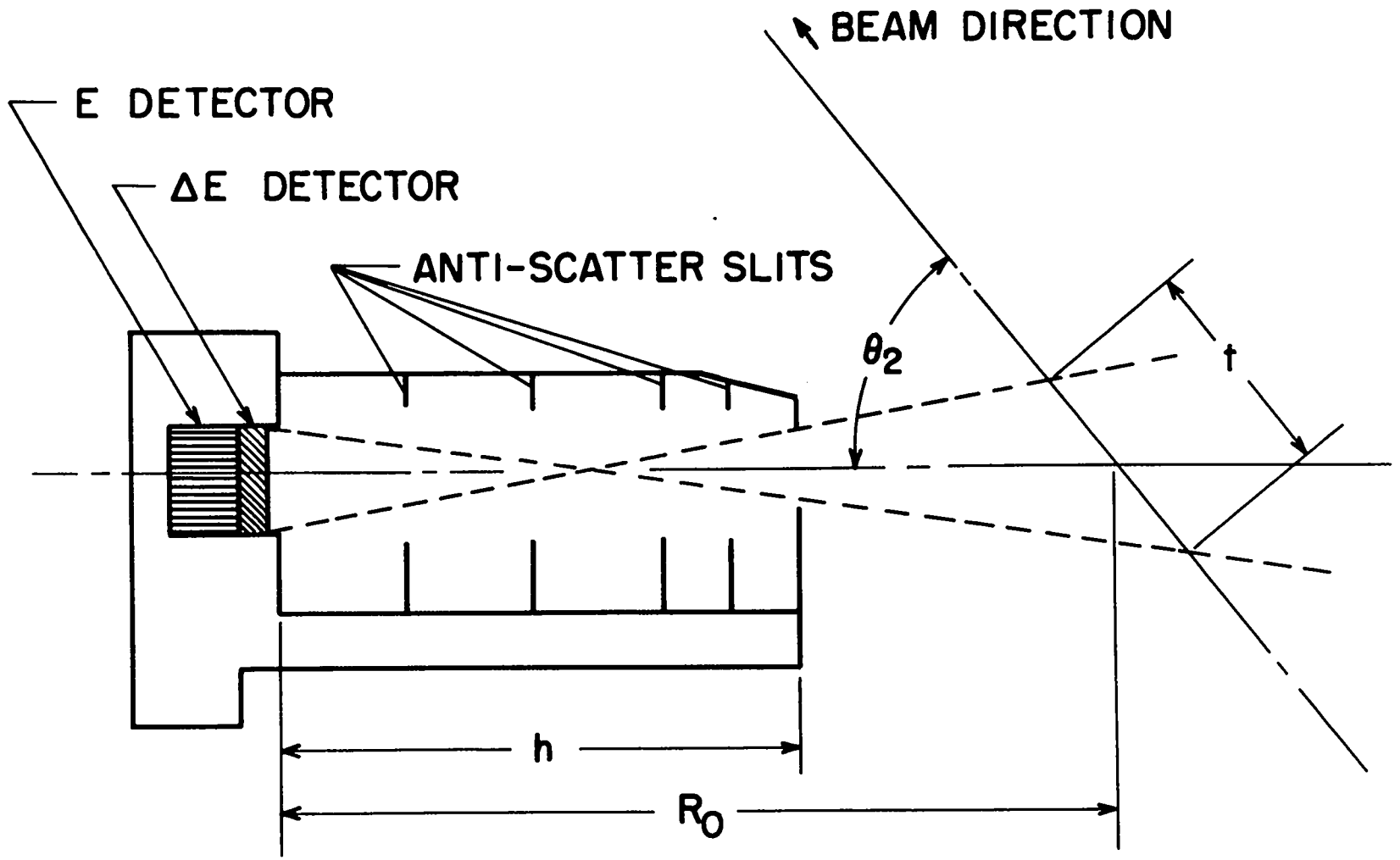

Fig. 5

To aid in mass discrimination, absorber foils could be placed either between the semiconductor detectors or immediately in front of the ΔE counter. The slit dimensions specified in Fig. 5 provided an angular resolution of ±4° (c.m.) for the second scattering.

Although corrections due to finite geometry were not made, measurements with smaller slits providing an angular resolution of ±2° (c.m.) yielded consistent results.

3.2d Electronics

A block diagram of the electronics used in the asymmetry measurements is shown in Fig. 6. Signals from each of the four E and ΔE detectors were taken into preamplifiers located immediately beneath the scattering chamber. Pulses from the 4 ΔE preamplifiers were then amplified, and fed into Cosmic discriminator units* equipped with pulse height discriminators and square pulse generators which were triggered by incoming pulses above the discriminator level. These square pulses provided information to the coincidence and routing box, which was used to identify the detector telescope in which a given event was detected. By adjusting the bias levels of the discriminators, it was possible to eliminate the unnecessary low energy pulses resulting from detector noise.

The signals emerging from the four ΔE and E preamplifiers were taken through separate mixers and the resulting summed signals fed into two Ortec** Model 210 amplifiers. The summed pulses, after

*Cosmic Radiation Labs., Inc. Model 801.

**Oak Ridge Technical Enterprises, Inc., Oak Ridge, Tennessee.

Figure 6. Block diagram of electronics.

BLOCK DIAGRAM OF ELECTRONICS FOR MASS DISCRIMINATION

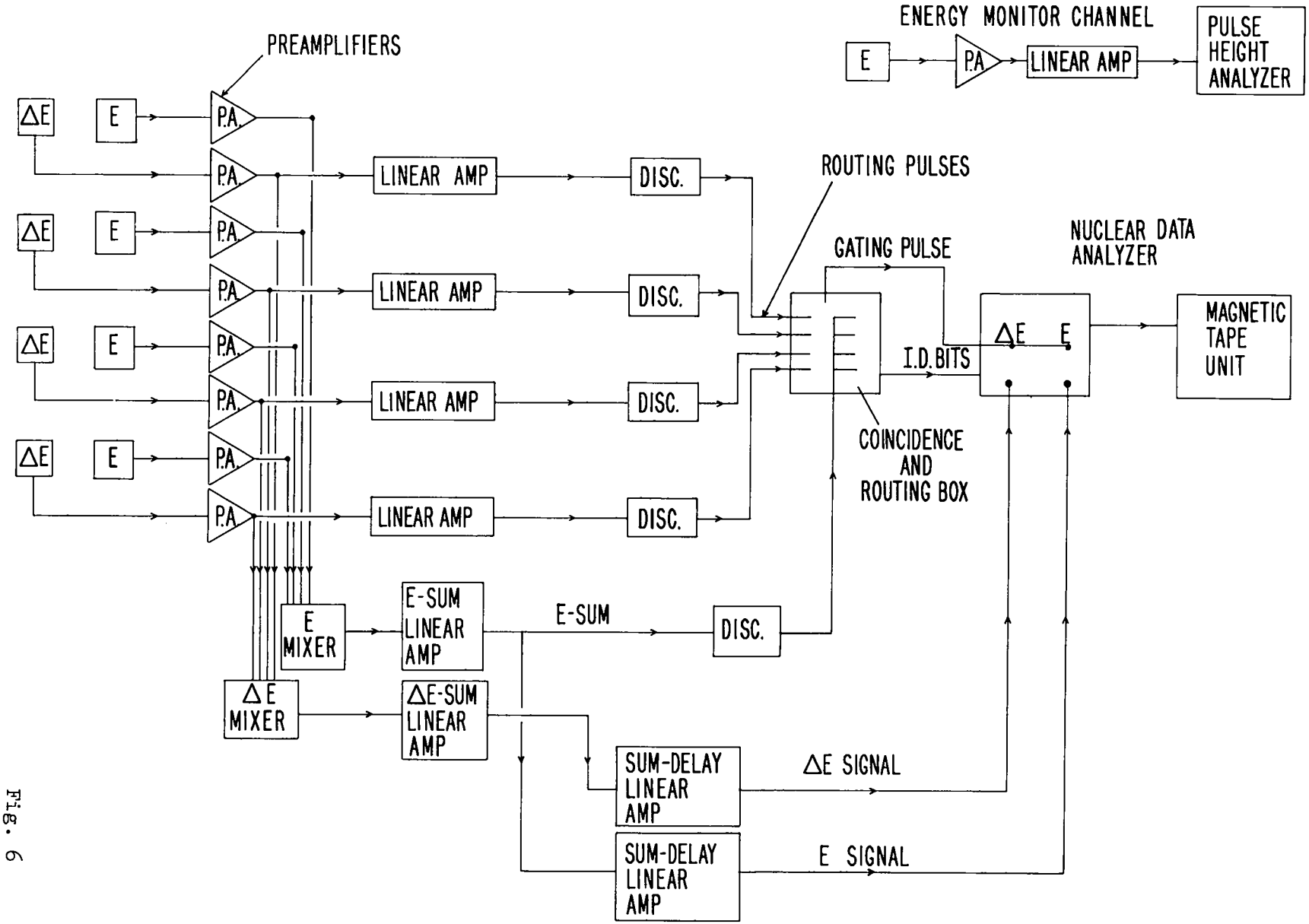

Fig. 6

being passed through delay lines, served as the ΔE and E signals to the Nuclear Data* analyzer. The E-sum signal was also used to generate a gating pulse to the routing box. The gating of the routing box was necessary in order to achieve coincidence conditions between the two detectors in the appropriate counter telescope. This coincidence requirement reduced the background to a negligible amount, except for a few back-angle measurements. When coincidence conditions had been met at the routing box, an additional gating pulse along with routing information was supplied the 4096 channel analyzer. Thus, the telescope designation along with the E and ΔE pulses were recorded event by event on magnetic tape with the 4096 channel analyzer acting as a buffer. Four 32×32 channel blocks of the analyzer were used to monitor the data, but the actual data was recorded with 256×256 channel resolution. The magnetic tape was processed off-line to produce two-dimensional ΔE vs E plots and tables for each telescope.

To insure that the routing system was operating properly, short runs were taken using a pulse generator, with three of the four mixer input lines disconnected, to check if any pulses from any particular quadrant were crossing over into the wrong quadrant. This procedure was repeated, for each of the four E counters. In addition, a 400-channel RIDL** pulse-height analyzer was used to monitor the energy of the secondary deuteron beam to insure that both scatterings were taking place at the desired energies. This procedure was also used in the adjustment of the primary alpha beam energy.

*Nuclear Data, Inc., Madison, Wisconsin.

**Radiation Instrument Development Laboratory, Inc.

3.3 Experimental Procedure

3.3a The Quantities of Interest

The experiment was performed with four detectors placed symmetrically about the secondary deuteron beam at azimuthal angles ϕ_2=0, 90, 180, and 270 degrees. The total counts recorded in each of these ϕ directions will be referred to as L, U, R, and D, respectively. Since the second scattering chamber was designed to be rotated about the beam axis, a measurement at a single angle θ_2 consisted of four runs with the chamber rotated through 90° after each run. Thus, with a, b, and c, as defined by Eq. (3.1), the following ratios become the quantities of interest:

$$\frac{R}{L} = \frac{(a+c)-b}{(a+c)+b} = \frac{(R_1R_2R_3R_4)^{1/4}}{(L_1L_2L_3L_4)^{1/4}} \tag{3.2}$$

and

$$\frac{U+D}{R+L} = \frac{a-c}{a+c} = \frac{(U_1U_2U_3U_4)^{1/4}+(D_1D_2D_3D_4)^{1/4}}{(R_1R_2R_3R_4)^{1/4}+(L_1L_2L_3L_4)^{1/4}} \tag{3.3}$$

where, for example, R_1 is the number of counts recorded in telescope 1 when it is to the right (ϕ_2=180°). The a's, b's, and c's in the above expressions are defined in Eq. (3.1).

By using the geometric mean values of the yields of particles scattered into the detectors, it was possible to eliminate the effects of different efficiencies for the various counters, solid angle differences, and differences in the total integrated current (Ha 63). It is also possible to eliminate the effects of small differences in the

second-scattering angles at which each detector is positioned, providing the unpolarized cross section is linear over the angular region involved.

Although it would be possible to measure more ratios than the two mentioned above (such as placing the counters at ϕ_2=45, 135, 225, and 315°), such measurements would not provide any additional information. This can be realized by recalling that a system of linear homogeneous equations in n unknowns has a non-trivial solution if and only if the rank of the system is less than n. Consequently, with only two independent ratios (b/a, c/a), it is only possible to formulate two linearly independent equations. Any third relation would be linearly dependent and would not provide any additional information. The angles of ϕ=0, 90, 180, and 270° were chosen because the largest asymmetry effects are present at these angles.

3.3b Data Collection and Reduction

Although four 32×32 channel blocks of the Nuclear Data two-dimensional analyzer were used to monitor the data, the actual data was recorded with 256×256 channel resolution. With this resolution, particle identification proved difficult for only a small number of measurements.

Data reduction was performed in large part with an IBM-7094 computer. Included in the computer output was a 35-mm film negative of a ΔE vs E plot for each counter telescope at each angle and rotational position. A selected plot of ΔE vs E is shown in Fig. 7. The computer output also included listing of the number of counts within

Figure 7. Plot of ΔE (rate of energy loss) versus E (energy of particle) for a particular counter telescope. The elastic deuteron group lies in region A, while protons from deuteron breakup are located in region B.

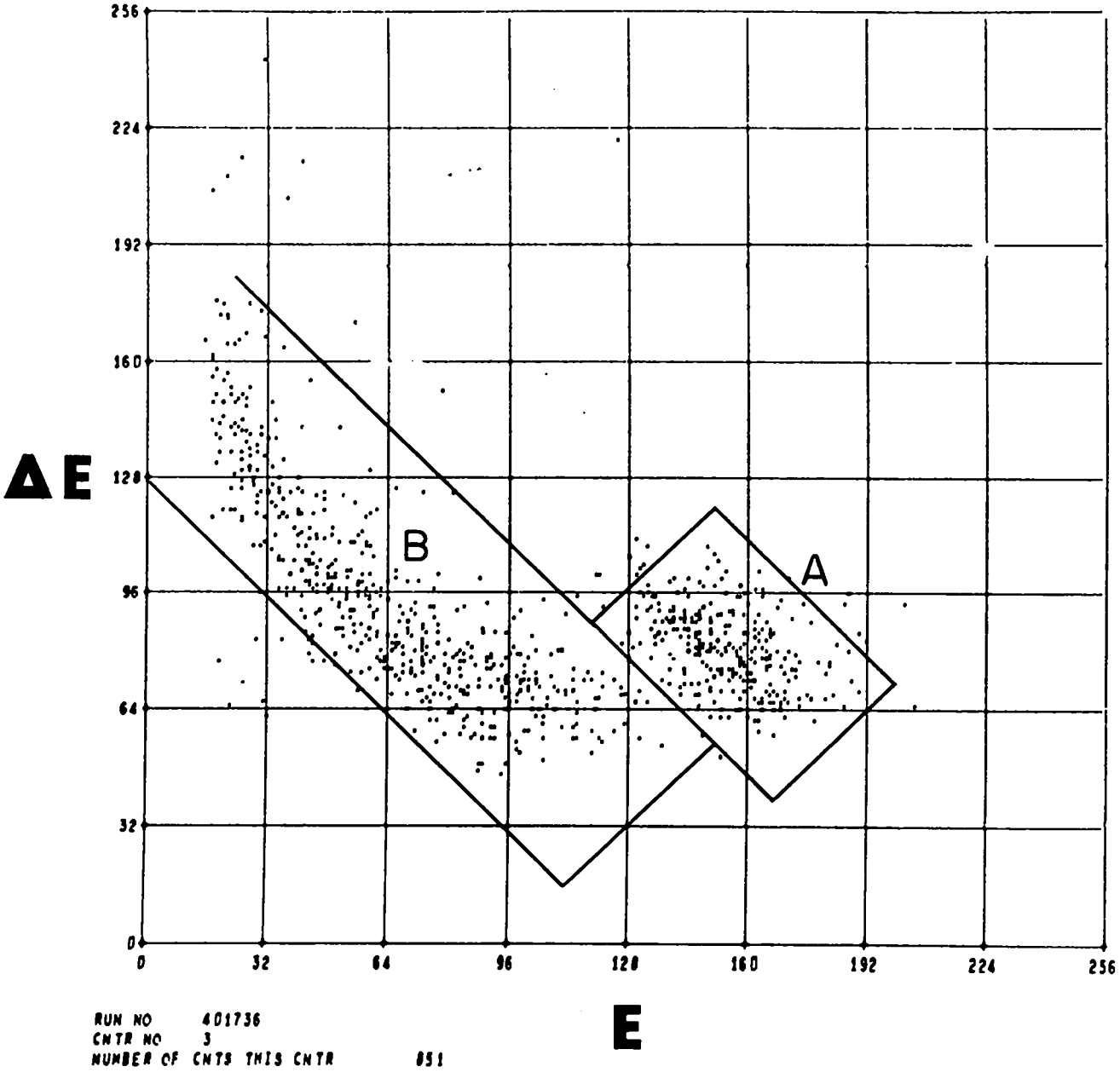
ΔE
E
256
224
192
160
128
96
64
32
0
0
32
64
96
128
160
192
224
256
A
B
RUN NO 401736
CNTR NO 3
NUMBER OF CNTS THIS CNTR 851

Fig. 7

a number of diagonal regions of these plots. The film could then be printed out and used to determine the region of interest (channel range and diagonal region) for every detector at every angle.

The average counting rates generally ran about 300 counts per hour per counter for a primary beam of 5 microamperes. After rotating the scattering chamber at the end of each run, the contents of the memory of the analyzer were recorded on photographic film (in 32×32 channel resolution). This procedure served for monitoring of the data quality.

3.3c Charge Collection

The total beam current was determined by integrating the total charge collected on an electrically insulated Faraday Cup positioned immediately behind the deuterium target (see Fig. 4). The current integration was determined to a relative accuracy of a few percent in order to be able to properly correct for the number of background counts.

3.3d Sources of Background

The main background contribution was due to neutrons from deuteron breakup in the first target and in the Havar foils. Although shielding was employed, a sufficient number of neutrons were able to penetrate the second-scattering chamber and initiate (n,α) reactions in either the ΔE or E silicon counter. Some of the resulting alpha particles could then cause a coincidence in the detector system and produce a recorded event. Other sources of background such as

scattering from foils and slit edges were minimized by the detector slit systems. A valve on the main beam tube was closed during the background runs to stop deuterons from entering the second-scattering chamber. Background was appreciable for only a few back angles, and in no case was the background correction to the measured asymmetries greater than 5%. Uncertainties due to the yields in the background as well as other sources of error will be discussed in section 3.4.

3.3e Alignment of the System

The asymmetry (Up plus Down) to (Right plus Left) is essentially independent of beam position and direction. On the other hand, since small deviations of the beam from the axis of the system could result in significant errors in the Right-to-Left ratio, an accurate alignment procedure had to be devised. Accordingly, the system was aligned by determining its angular position by Right-to-Left deuteron-gold elastic scattering measurements and then determining the relative position of the beam by means of nuclear emulsions placed at the center of the second-scattering chamber.

This alignment procedure is justified, since the differential cross section measurements of Igo et al. (Ig 61) with 11.8-MeV deuterons indicate that the d-Au scattering cross section is Rutherford up to an angle of 50°. The angle determination procedure is highly accurate since the Rutherford cross section varies by as much as 40% per degree at the far forward angles. However, because of machine instability, the beam position measurements were limited to an accuracy of ±0.016 inch. This restriction, in turn, limited the angular alignment of

the second-scattering chamber to the value quoted below.

The Right-to-Left d-Au measurements were made with a 5-mg/cm^2 gold foil positioned at the center of the second-scattering chamber. During the alignment runs, the second-scattering chamber was evacuated and the detector slit assemblies were removed. Removing the detector slit systems enhanced the counting rate without appreciably affecting the angular resolution, since, for a solid target, the latter quantity is determined mainly by the size of the detector aperture. Alpha particles elastically scattered from the Havar foils of the first target could easily be distinguished from the elastically scattered deuterons on the basis of the observed pulse-height spectra. After the data were collected, the alignment was again checked by repeating the Right-to-Left d-Au measurements at several second-scattering angles.

A primary beam of 2 μa was sufficient to provide approximately 1000 counts/min in each detector and to allow the alignment runs to be made with a statistical accuracy approaching 1%.

3.4 Uncertainties

3.4a Alignment Uncertainties

The second-scattering chamber was limited to within 0.20° of being perfectly aligned because of false asymmetries arising from the energy and intensity variations of the incident deuteron beam across the entrance to the second-scattering chamber. Such effects produced a shift in the effective center of the second target and

resulted in an error in the Right-to-Left asymmetry as large as ±0.03 for angles smaller than 60° (c.m.) but nor more than ±0.01 for the remaining angles.

3.4b Statistical Uncertainties

Additional uncertainties in the measurements resulted from uncertainties in the counter yields. A sufficient number of counts were recorded at each datum point to determine the counter yields to a statistical accuracy of between 3% and 5%. In many instances, data points were remeasured to obtain an average of two measurements and thereby reduce the statistical uncertainty. The major contribution to the uncertainties in the measured asymmetries is of a statistical nature.

3.4c Other Uncertainties

In no instance was the background correction to the measured asymmetries greater than 5%. However, because of low background counting rates, it was infeasible to determine the background to a statistical accuracy of better than 10%. This was the dominant source of error in the background measurements and introduced an additional 0.5% uncertainty in the measured asymmetries, although appropriate corrections were only applied in those instances in which this uncertainty would be a significant contribution to the total error.

In view of the well-defined spectra obtained in each detector at nearly every angle, multiple scattering and slit edge scattering effects were considered to be an insignificant contribution to the

total error.

On the basis of a discussion by Satchler (Sa 60), it was concluded that the secondary beam polarization was not appreciably affected while passing through the magnetic fields of the quadrupole focusing lens. Accordingly, these effects were ignored.

According to Wolfenstein's calculations (Wo 49) for 7-MeV protons stopped in foil, the slowing down process does not significantly affect the polarization (i.e., there is an effect of about one part in 10^5). Consequently, it was assumed that the slowing process did not affect the deuteron polarization.

The sources of error and the corresponding errors in the asymmetry measurements are summarized in Table I. The error quoted for the beam alignment and machine instability is for angles greater than 60° (c.m.).

TABLE I

ERRORS IN DEUTERON-ALPHA ASYMMETRY MEASUREMENTS

Source of Error	% Error
Cyclotron instability and beam alignment	2.0%
Background uncertainty	0.5%
Statistical uncertainty	3%-8%

3.5 Experimental Results

The results of the measurements of the asymmetries Right-to-Left and (Up plus Down) to (Right plus Left) for d-^{4}He double scattering are shown in Figs. 8 and 9 and are listed in Table II. For the data presented in Fig. 8, both scatterings take place at the same center-of-mass energy, which corresponds to an equivalent deuteron energy of 9.0 MeV. Deuterons from the first target recoiling from alpha-particle bombardment at a laboratory angle of 29.15° (122° c.m.) were slowed with absorber foils (so that both scatterings took place at the same center-of-mass energy) and scattered from a ^{4}He gas target. The asymmetries were measured for nine second-scattering angles between 45° and 105° center-of-mass. Statistical errors as quoted in Table II are about ±0.04 to ±0.06 for R/L and ±0.02 to ±0.04 for (U+D)/(R+L). These numbers generally characterize the statistical uncertainties of the results presented in Table II and Figs. 8-10, although uncertainties which differ from these by a factor of two may be found. Values of R/L and (U+D)/(R+L) as low as 0.739±0.028 and 0.813±0.017 respectively were observed.

As shown in Fig. 10, the results appear to be in excellent agreement with subsequent measurements taken at the University of Wisconsin with a polarized-ion source (Lo 67).

Further asymmetry measurements for 11.0-MeV deuterons (second scattering) are also presented in Table II and shown in Fig. 9. As in the previous case, the energy of the first scattering corresponded to 9.0-MeV deuterons (i.e., 18-MeV alpha particles). The measurements

TABLE II

MEASURED AZIMUTHAL ASYMMETRIES

E_d(lab) for second scattering (MeV)	θ_2(c.m.)	Right / Left	Up plus Down / Right plus Left
9.0	44.57	1.016±0.037	---
9.0	51.78	1.091±0.045	---
9.0	58.87	1.244±0.052	1.078±0.031
9.0	65.84	1.520±0.070	1.023±0.033
9.0	69.96	1.355±0.053	0.911±0.025
9.0	79.34	1.175±0.042	0.879±0.023
9.0	85.83	1.051±0.039	0.866±0.024
9.0	92.13	0.969±0.030	0.841±0.019
9.0	104.08	0.739±0.028	0.813±0.017
11.0	44.57	0.920±0.030	---
11.0	51.78	0.875±0.030	---
11.0	58.87	0.842±0.036	1.144±0.033
11.0	65.84	1.046±0.038	0.929±0.025
11.0	69.96	1.109±0.049	0.939±0.030
11.0	72.68	1.214±0.041	0.855±0.021
11.0	79.34	1.150±0.042	0.875±0.023
11.0	85.84	1.082±0.047	0.866±0.027
11.0	93.37	0.956±0.030	0.819±0.019
11.0	104.08	0.802±0.028	0.818±0.021
11.0	114.03	0.753±0.031	0.826±0.025
11.0	118.19	0.633±0.026	0.843±0.026

An angular resolution of ±4° (c.m.) was used at both energies.

Figures 8 and 9. The azimuthal asymmetries Right-to-Left and (Up plus Down) to (Right plus Left) for d-^{4}He double scattering. For the data shown in Fig. 8, the second scattering takes place at 9.0-MeV deuteron energy. For the results presented in Fig. 9, the second scattering occurs at 11.0-MeV deuteron energy. Both first and second scatterings take place at the same center-of-mass energy which corresponds to 9.0-MeV deuterons (i.e., 18-MeV alpha particles). The first-scattering angle is designated.

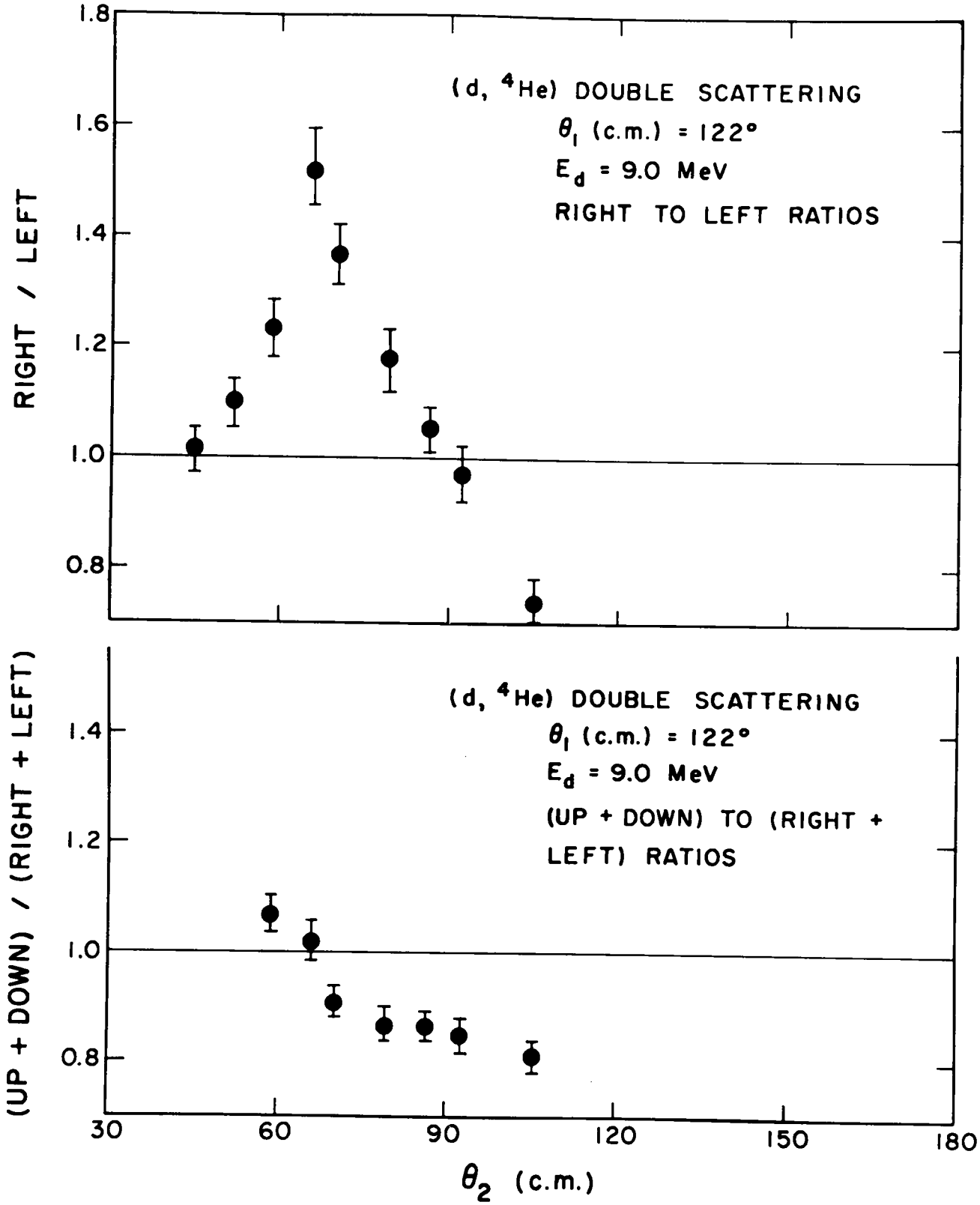
(d, 4He) DOUBLE SCATTERING
θ1 (c.m.) = 122°
Ed = 9.0 MeV
RIGHT TO LEFT RATIOS
RIGHT / LEFT
1.8
1.6
1.4
1.2
1.0
0.8
(d, 4He) DOUBLE SCATTERING
θ1 (c.m.) = 122°
Ed = 9.0 MeV
(UP + DOWN) TO (RIGHT + LEFT) RATIOS
(UP + DOWN) / (RIGHT + LEFT)
1.4
1.2
1.0
0.8
30
60
90
120
150
180
θ2 (c.m.)

Fig. 8

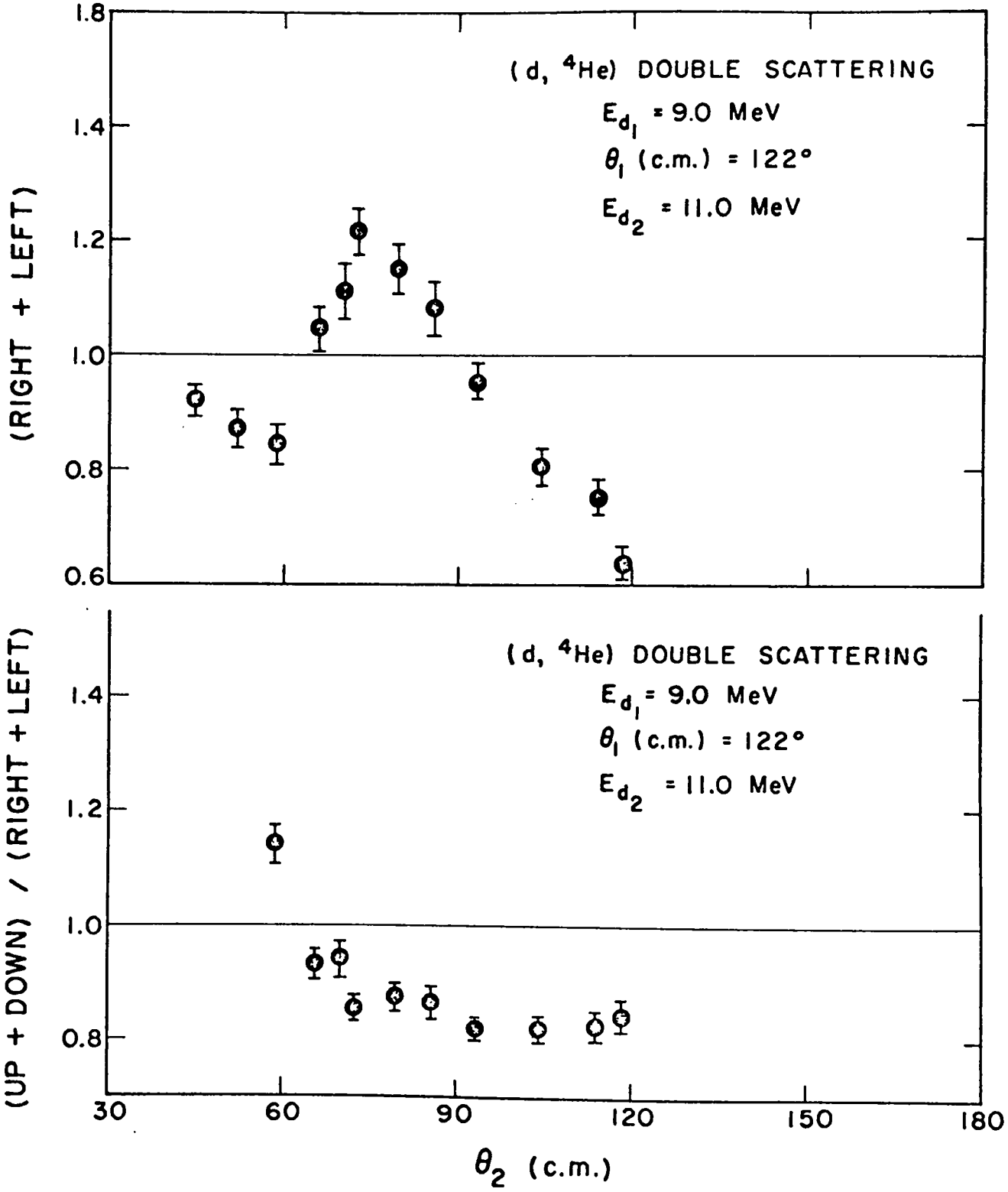
(d, 4He) DOUBLE SCATTERING
Ed1 = 9.0 MeV
θ1 (c.m.) = 122°
Ed2 = 11.0 MeV
(RIGHT + LEFT)
1.8
1.4
1.2
1.0
0.8
0.6
(d, 4He) DOUBLE SCATTERING
Ed1 = 9.0 MeV
θ1 (c.m.) = 122°
Ed2 = 11.0 MeV
(UP + DOWN) / (RIGHT + LEFT)
1.4
1.2
1.0
0.8
30
60
90
120
150
180
θ2 (c.m.)

Fig. 9

Figure 10. Comparison of the results of the present experiment with those subsequently obtained (triangles) with a polarized-ion source at the University of Wisconsin (Lo 67). The solid curve is a line drawn through the data points.

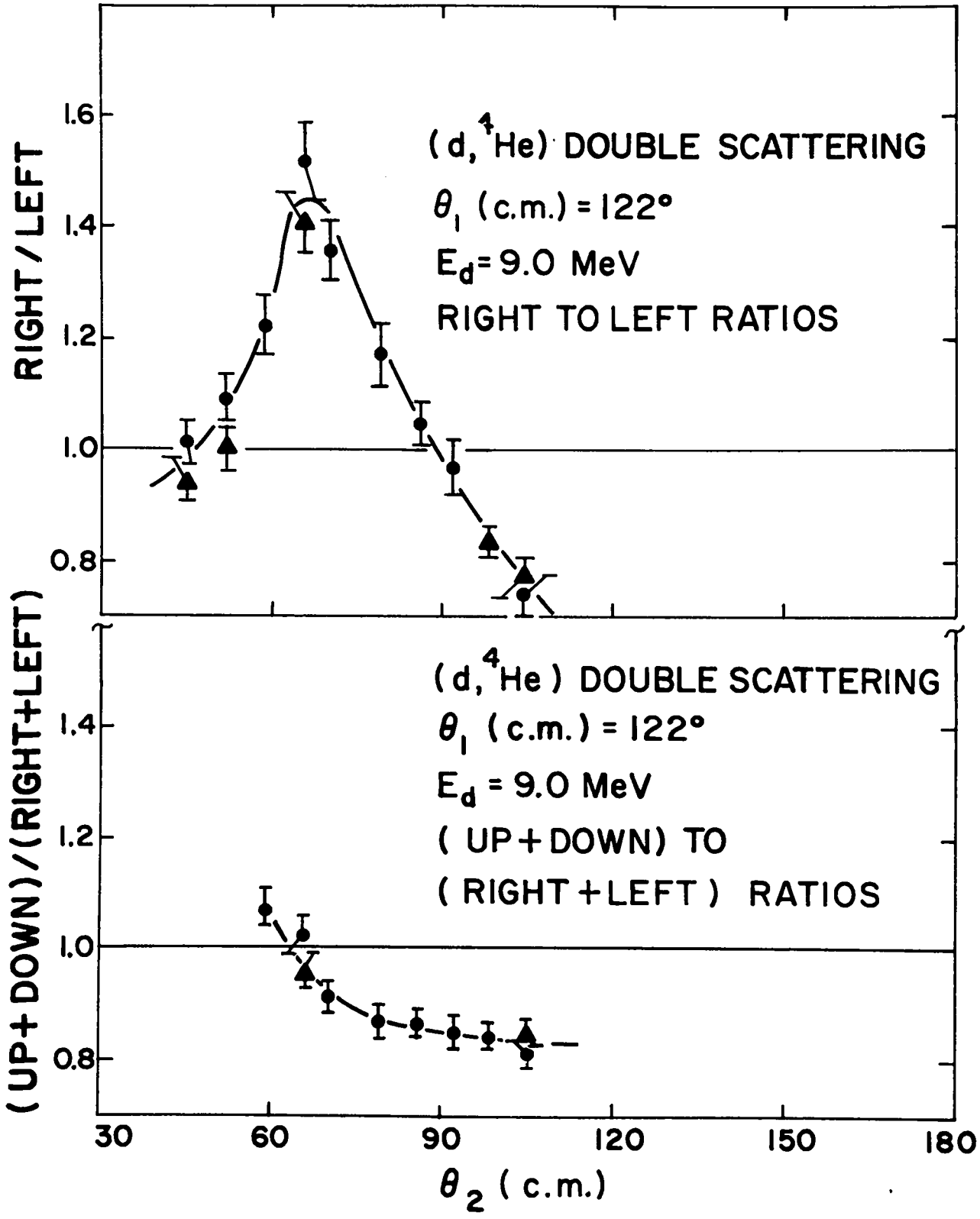
RIGHT / LEFT
1.6
1.4
1.2
1.0
0.8
(d, ⁴He) DOUBLE SCATTERING
θ1 (c.m.) = 122°
Ed = 9.0 MeV
RIGHT TO LEFT RATIOS
(UP+DOWN)/(RIGHT+LEFT)
1.4
1.2
1.0
0.8
(d, ⁴He) DOUBLE SCATTERING
θ1 (c.m.) = 122°
Ed = 9.0 MeV
(UP+DOWN) TO
(RIGHT+LEFT) RATIOS
30
60
90
120
150
180
θ2 (c.m.)

Fig. 10

were made for 12 second-scattering angles between 45° and 118° (c.m.). Values of R/L as low as 0.633±0.026 were observed at 118° (c.m.).

3.6 Discussion

Figure 11 illustrates the results obtained at 9.0 MeV (both scatterings) together with the predictions from the phase shifts obtained by McIntyre and Haeberli (Mc 65). The agreement between the predicted and measured asymmetries is poor. It should be pointed out that the asymmetries are essentially proportional to the spin tensor moments which characterize the first scattering. Thus, small changes in the phase shifts can produce a large change in the scale factor without appreciably changing the shape of the curves. For example, although the predicted values of (U+D)/(R+L) are all within 0.1% of unity, the shape of the curve is nevertheless similar to the observed curve.

Figure 12 shows the values of $\langle iT_{11}\rangle_2$ extracted from the data of Fig. 8. Several assumptions must be made in order to do this: 1) the beam polarization $\langle iT_{11}\rangle_1$ was determined to be -0.26 by normalization to measurements of McIntyre (Mc 66) and Trier (Tr 67); 2) $\langle T_{21}\rangle_1\langle T_{21}\rangle_2$ is small compared to $\langle iT_{11}\rangle_1\langle iT_{11}\rangle_2$; 3) $\langle T_{20}\rangle_1\langle T_{20}\rangle_2$ is small compared to one. With these approximations, which are consistent with all available data (Se 64, Mc 66, Mc 67a, Mc 67b, Tr 67), we can write

Figure 11. Results of the present experiment together with the predictions based on the phase shifts of McIntyre and Haeberli (Mc 65).

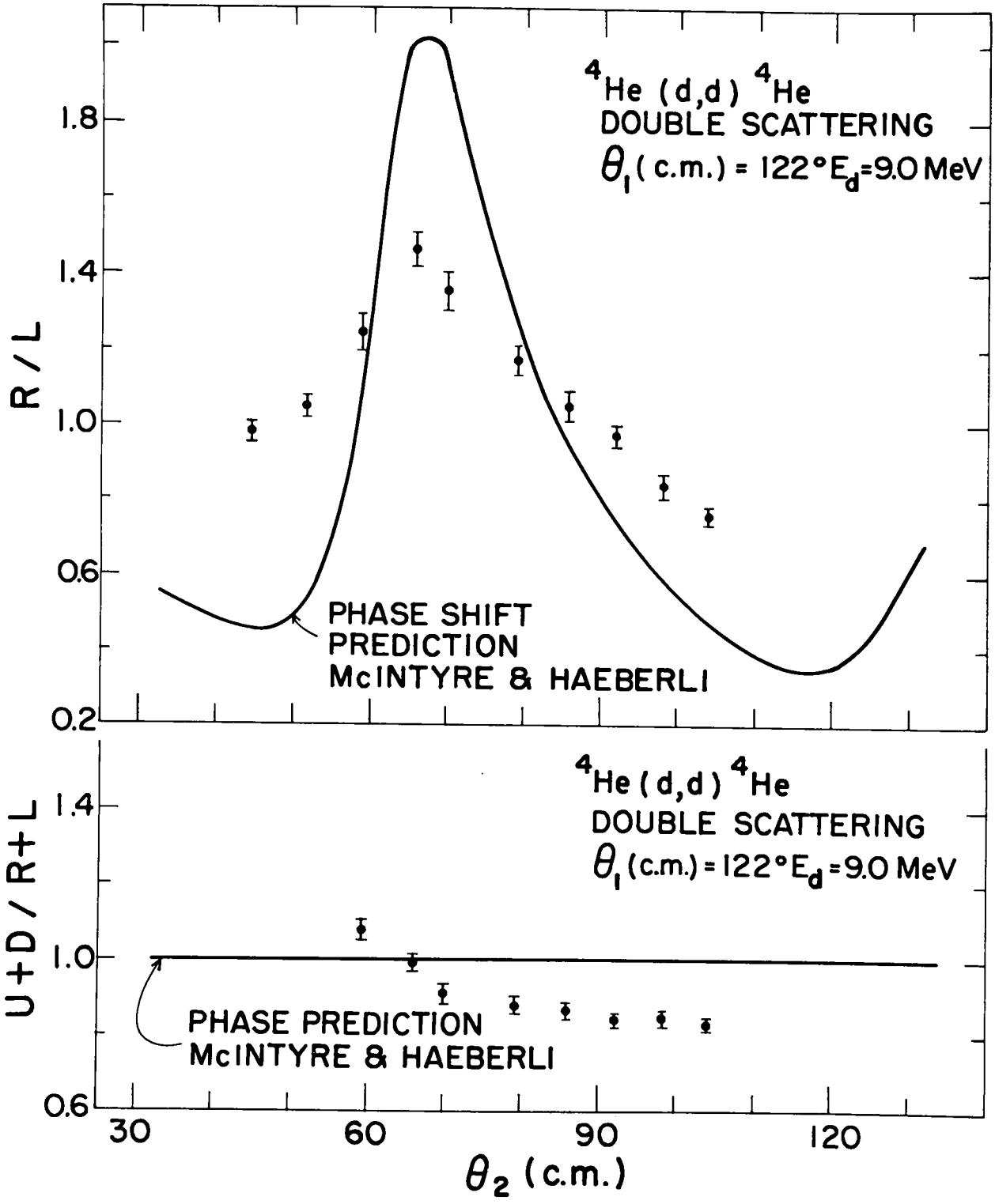
^{4}He (d,d) ^{4}He
DOUBLE SCATTERING
θ_1 (c.m.) = 122° E_d = 9.0 MeV
R / L
1.8
1.4
1.0
0.6
0.2
PHASE SHIFT
PREDICTION
McINTYRE & HAEBERLI
^{4}He (d,d) ^{4}He
DOUBLE SCATTERING
θ_1 (c.m.) = 122° E_d = 9.0 MeV
U+D / R+L
1.4
1.0
0.6
PHASE PREDICTION
McINTYRE & HAEBERLI
30
60
90
120
θ_2 (c.m.)

Fig. 11

Figure 12. Comparison of the results of the present experiment with the measurements of Trier et al. (Tr 67), and the theoretical predictions of Senhouse et al. (Se 64b) and McIntyre et al. (Mc 65). The vector polarization $\langle iT_{11} \rangle_1$ due to the first scattering is indicated.

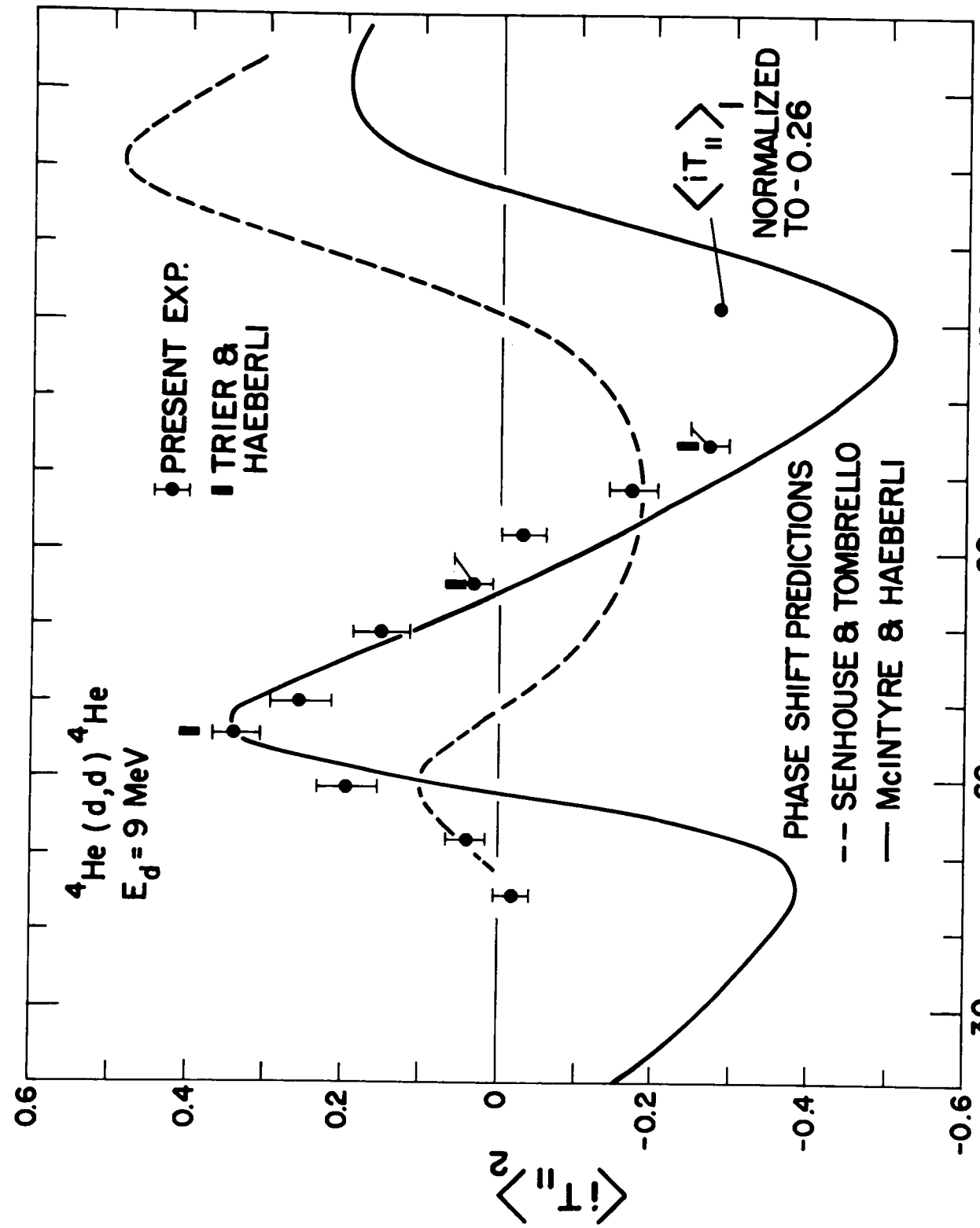
^{4}He (d,d) ^{4}He
E_d = 9 MeV
PRESENT EXP.
TRIER & HAEBERLI
PHASE SHIFT PREDICTIONS
-- SENHOUSE & TOMBRELLO
— McINTYRE & HAEBERLI
$\langle iT_{11} \rangle_1$ NORMALIZED TO -0.26
$\langle iT_{11} \rangle_2$
θ_2 (c.m.)
0.6
0.4
0.2
0
-0.2
-0.4
-0.6
30
60
90
120
150

Fig. 12

$$\langle iT_{11}\rangle_2 = \frac{1}{0.26}\left[\frac{R-L}{R+L+U+D}\right] * \qquad (3.4)$$

from which Fig. 12 and Table III were prepared. Thus, even when the data are presented in the form of Eq. (3.4) where most of the sensitivity to the first-scattering tensors is removed, agreement between the available predictions and the data is poor.

The conclusions to be drawn from this investigation are that the results appear to be in excellent agreement with subsequent measurements made at the University of Wisconsin with a polarized-ion source. In addition, phase-shift predictions based on these measurements are consistent with the phase predictions of Trier et al. (Tr 67) at lower deuteron energies. However, it was necessary to include a small F-wave contribution in the present analysis in order to achieve excellent fits to the data. These measurements have demonstrated that a deuteron beam with useful vector polarization can be produced by deuteron-alpha elastic scattering at energies near 10 MeV.

On the basis of these measurements it was decided to change the first scattering angle to 31° (118° c.m.) and raise the equivalent deuteron energy to 11.5 MeV (i.e., 23-MeV alpha particles). This procedure produced a secondary beam of 14.0-MeV deuterons and represented the highest energy at which the experiment could have been

---

*The polarization $\langle iT_{11}\rangle_1 = -0.26$ is slightly smaller than the value -0.28 quoted by Bernstein et al. (Be 67), which was based on earlier Wisconsin measurements.

feasibly performed on the LAVEC. The results and significance of the ensuing experiments are discussed in later chapters.

TABLE III

VECTOR POLARIZATION FOR 9.0-MeV DEUTERON ENERGY

E_d(lab) for second scattering (MeV)	θ_2(lab)	θ_2(c.m.)	$\langle iT_{11} \rangle_2$
9.0	30.00	44.57	-0.018±0.023
9.0	35.00	51.78	0.041±0.025
9.0	40.00	58.87	0.196±0.040
9.0	45.00	65.84	0.338±0.033
9.0	48.00	69.96	0.257±0.039
9.0	55.00	79.34	0.153±0.037
9.0	60.00	85.83	0.032±0.025
9.0	65.00	92.13	-0.031±0.029
9.0	70.00	98.22	-0.171±0.032
9.0	75.00	104.08	-0.270±0.025

CHAPTER IV

DEUTERON-ALPHA POLARIZATION MEASUREMENTS AS AN AID IN ION SOURCE CALIBRATION

4.1 Introduction

In view of the rapid development of polarized-ion source techniques during the past few years, improved methods for the absolute calibration of the polarization produced by such sources have become highly desirable. The $^{3}He(d,p)^{4}He$ and $T(d,n)^{4}He$ reactions when excited with S-wave deuterons have generally been considered to be an acceptable means of measuring deuteron tensor polarization. However, it has been established (Br 66) that the reactions proceed with both S=3/2 and S=1/2 channel spins. Consequently, the absolute analyzing power of these reactions is uncertain. For absolute determination of deuteron tensor polarization, the use of (d,α) reactions on $J^{\pi}=0^{+}$ target nuclei leading to a $J^{\pi}=0^{+}$ residual nucleus have been suggested (Ja 61), because for this type of reaction the analyzing power is predicted uniquely without reference to the particular reaction process. Unfortunately, because of the isobaric spin selection rule, reactions of this kind proceed with rather small intensity. Prior to the present work, no absolute analyzer for deuteron vector polarization has been available. Consequently, it was felt to be useful to demonstrate that azimuthal asymmetries produced in d-^{4}He double scattering at 11.5-MeV deuteron energy (both scatterings) can be used to provide an independent and absolute calibration for the vector

polarization of a beam of deuterons produced by a polarized-ion source.

On the basis of extensive phase analysis of the results of the d-^{4}He polarization measurements discussed in the preceding chapter, it was concluded that larger deuteron vector polarization effects could be obtained if the first-scattering angle were increased from 29° to 31° (118° c.m.) and if the equivalent deuteron energy for both scatterings were raised from 9.0 to 11.5 MeV (i.e., 23-MeV alpha particles). Because of the actual magnitudes of the various tensor parameters, this method provides primarily (at the energy and angle used here) a vector polarization calibration.

4.2 Asymmetry Measurements for Ion Source Calibration

Following the experimental procedure outlined in Chapter III, measurements were made of the azimuthal asymmetries 1) Right-to-Left and 2) (Up plus Down) to (Right plus Left) for d-^{4}He double scattering. For the results presented in Fig. 13 and Table IV, both scatterings take place at the same center-of-mass energy, which corresponds to 11.5-MeV deuterons. The asymmetries were measured for 19 second-scattering angles between 45° and 126° (c.m.). Statistical errors as quoted in Table IV are about ±0.021 to ±0.046 for R/L and ±0.017 to ±0.040 for (U+D)/(R+L). As shown in Fig. 13, larger asymmetries have been obtained in the region of interest near 118° (c.m.), as was predicted by the phase analysis of earlier measurements.

Additional asymmetry measurements for 14.0-MeV deuterons (second scattering) are presented in Table IV and are shown in Fig. 14. As in the previous case, the energy of the first scattering corresponded

TABLE IV

MEASURED AZIMUTHAL ASYMMETRIES

E_d(lab) for second scattering (MeV)	θ_2(c.m.)	$\frac{\text{Right}}{\text{Left}}$	$\frac{\text{Up plus Down}}{\text{Right plus Left}}$
11.5	44.57	0.911±0.031	---
11.5	50.34	0.764±0.034	---
11.5	56.05	0.646±0.031	1.232±0.040
11.5	61.68	0.856±0.035	1.054±0.030
11.5	67.22	1.058±0.041	0.822±0.024
11.5	72.68	1.206±0.046	0.872±0.024
11.5	78.02	1.035±0.037	0.824±0.022
11.5	83.26	1.082±0.038	0.817±0.021
11.5	88.38	1.003±0.036	0.800±0.022
11.5	93.37	0.906±0.029	0.824±0.020
11.5	98.22	0.869±0.027	0.796±0.018
11.5	102.93	0.765±0.023	0.780±0.017
11.5	107.49	0.732±0.026	0.836±0.022
11.5	111.89	0.713±0.023	0.834±0.020
11.5	116.13	0.608±0.021	0.861±0.023
11.5	118.19	0.627±0.025	0.877±0.025
11.5	120.22	0.591±0.023	0.878±0.025
14.0	44.57	0.828±0.030	---
14.0	50.34	0.583±0.026	---
14.0	56.05	0.394±0.019	1.169±0.036
14.0	61.68	0.536±0.022	1.111±0.031
14.0	67.22	1.011±0.037	0.922±0.024
14.0	72.68	1.015±0.038	0.875±0.024
14.0	78.02	1.026±0.036	0.855±0.022
14.0	83.26	1.137±0.041	0.830±0.022
14.0	88.38	1.003±0.035	0.817±0.022

TABLE IV (continued)

MEASURED AZIMUTHAL ASYMMETRIES

E_d(lab) for second scattering (MeV)	θ_2(c.m.)	$\frac{\text{Right}}{\text{Left}}$	$\frac{\text{Up plus Down}}{\text{Right plus Left}}$
14.0	93.37	0.895±0.029	0.843±0.020
14.0	98.22	0.850±0.023	0.818±0.016
14.0	102.93	0.815±0.024	0.818±0.018
14.0	107.49	0.767±0.023	0.818±0.018
14.0	111.89	0.637±0.022	0.818±0.021
14.0	116.13	0.633±0.022	0.820±0.021
14.0	118.19	0.607±0.022	0.863±0.023
14.0	120.22	0.596±0.025	0.951±0.028
14.0	122.19	0.674±0.026	0.838±0.024
14.0	124.13	0.632±0.026	0.881±0.026
14.0	126.96	0.675±0.035	0.962±0.035
14.0	129.71	0.679±0.042	0.922±0.041
14.0	133.23	0.894±0.067	1.126±0.058

Figure 13. Azimuthal asymmetries Right-to-Left and (Up plus Down) to (Right plus Left) for d-^{4}He double scattering. Both scatterings take place at the same center-of-mass energy, which corresponds to 11.5-MeV deuterons. The center-of-mass first-scattering angle is indicated.

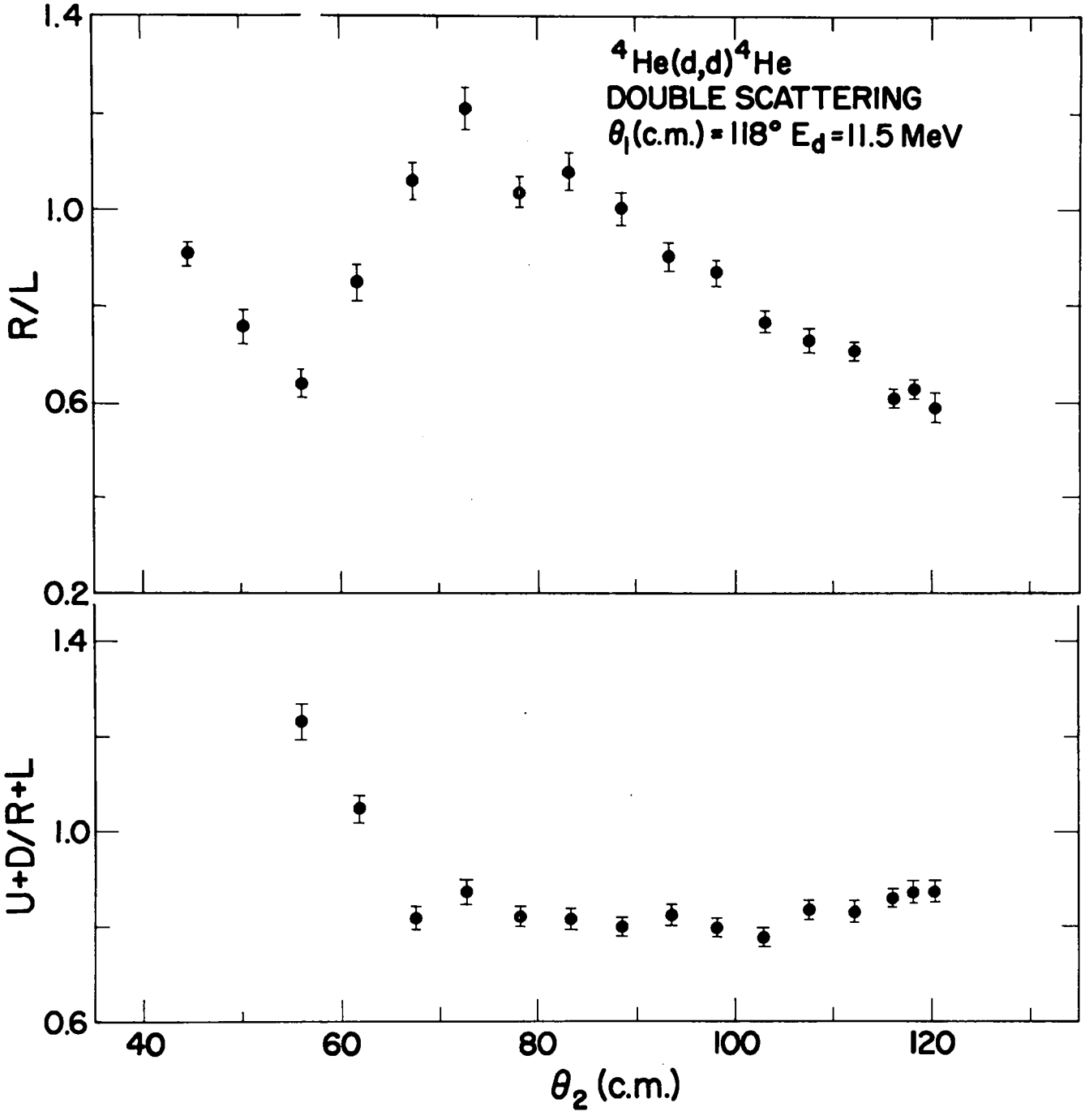
^{4}He(d,d)^{4}He
DOUBLE SCATTERING
θ_1(c.m.) = 118° E_d = 11.5 MeV
R/L
U+D/R+L
θ_2 (c.m.)
1.4
1.0
0.6
0.2
40
60
80
100
120

Fig. 13

Figure 14. Azimuthal asymmetries Right-to-Left and (Up plus Down) to (Right plus Left) for 14.0-MeV deuterons. The energy of the first scattering corresponds to 11.5-MeV deuterons. The first-scattering angle corresponds to 118° (c.m.).

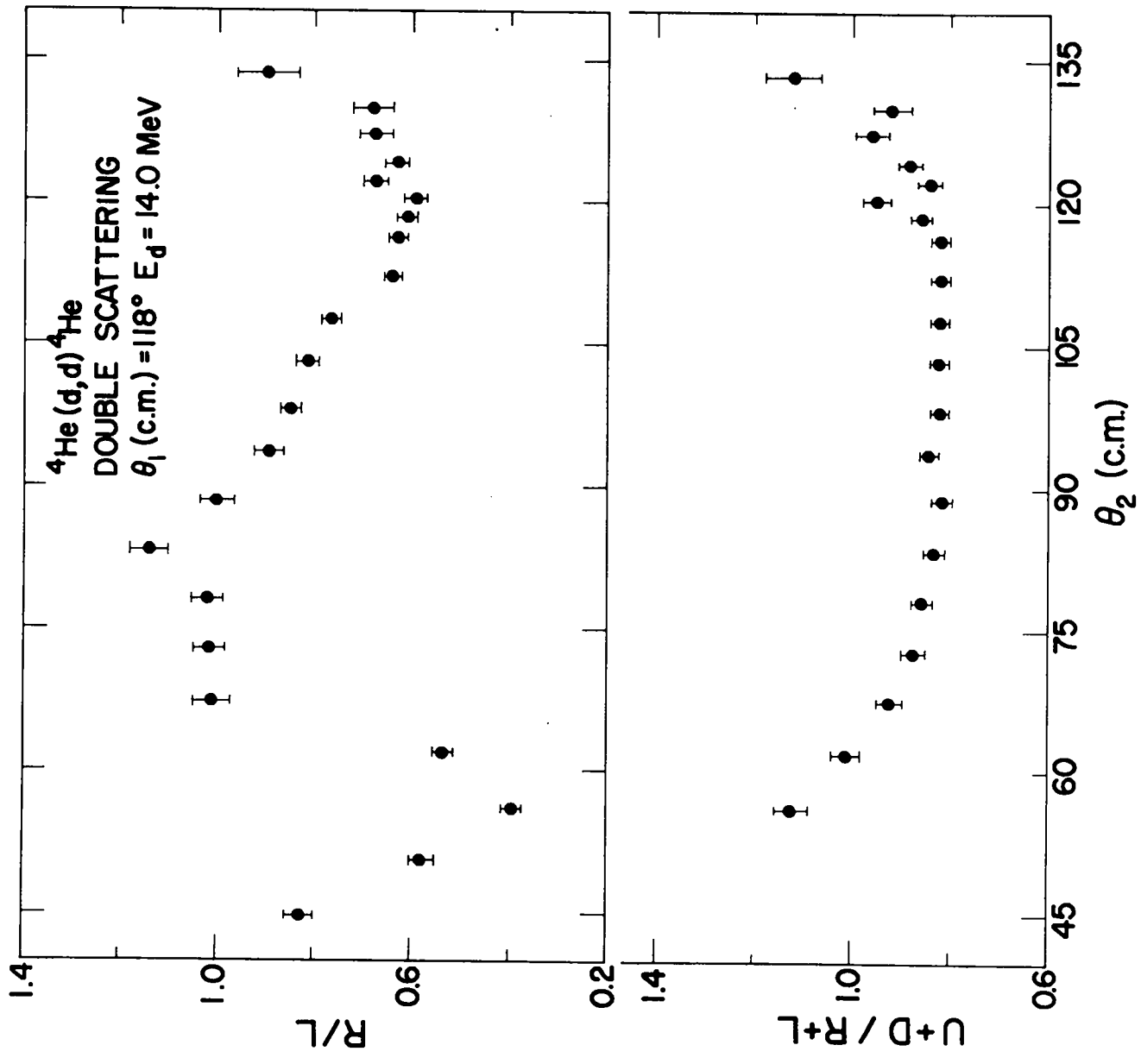
^{4}He(d,d)^{4}He
DOUBLE SCATTERING
θ_1 (c.m.) = 118° E_d = 14.0 MeV
R/L
U+D / R+L
θ_2 (c.m.)
1.4
1.0
0.6
0.2
45
60
75
90
105
120
135

Fig. 14

to 11.5-MeV deuterons. The measurements were made for 22 second-scattering angles between 45° and 135° (c.m.). A value of R/L of 0.607±0.022 was observed at θ_2=118° (c.m.).

Of particular interest is the asymmetry measurement at $\theta_1=\theta_2=118°$ for an equivalent deuteron energy of 11.5 MeV (both scatterings). Under proper rotation, the tensors involved in the description of this measurement are identical. Employing the approximations previously used in Chapter III, it becomes possible to determine the vector polarization of the secondary beam without relying upon normalization to previously existing measurements. The vector polarization was found to be $\langle iT_{11}\rangle_1=-0.360\pm0.015$, or 42% of its maximum possible value. Thus, a deuteron beam with useful vector polarization can be obtained from d-^{4}He elastic scattering in the 11.5-MeV deuteron energy range. Values of $\langle iT_{11}\rangle_2$ for a range of second-scattering angles are presented in Table V and Fig. 15.

4.3 Application of Asymmetry Measurements

As discussed in previous chapters, the polarization P in the spin-1/2 case may be completely determined from a measured Right-to-Left asymmetry, whereas in the spin-one case, there are four unknown tensor moments but only two independently measurable asymmetries. Thus, in general, the tensor parameters cannot be completely determined by double scattering. The measured asymmetries may nevertheless be used to provide an absolute calibration for a polarized beam which has been produced by a polarized-ion source and accelerated to 11.5 MeV. Of particular significance for ion source calibration purposes

TABLE V

VECTOR POLARIZATION FOR 11.5-MeV DEUTERON ENERGY

E_d(lab) for second scattering (MeV)	θ_2(lab)	θ_2(c.m.)	$\langle iT_{11} \rangle_2$
11.5	30.00	44.57	-0.130±0.031
11.5	34.00	50.34	-0.375±0.030
11.5	38.00	56.05	-0.272±0.031
11.5	42.00	61.68	-0.105±0.029
11.5	46.00	67.22	0.042±0.029
11.5	50.00	72.68	0.140±0.030
11.5	54.00	78.02	0.028±0.025
11.5	58.00	83.26	0.060±0.025
11.5	62.00	88.38	0.001±0.025
11.5	66.00	93.37	-0.075±0.025
11.5	70.00	98.22	-0.110±0.024
11.5	74.00	102.93	-0.210±0.025
11.5	78.00	107.49	-0.238±0.028
11.5	82.00	111.89	-0.260±0.025
11.5	86.00	116.13	-0.370±0.030
11.5	90.00	120.22	-0.385±0.033

Figure 15. Values of the vector polarization over a range of second-scattering angles as extracted from the data of Fig. 13. The solid curve is a theoretical prediction obtained from a phase-shift analysis employing the results of the present experiment. The vector polarization due to the first scattering is indicated.

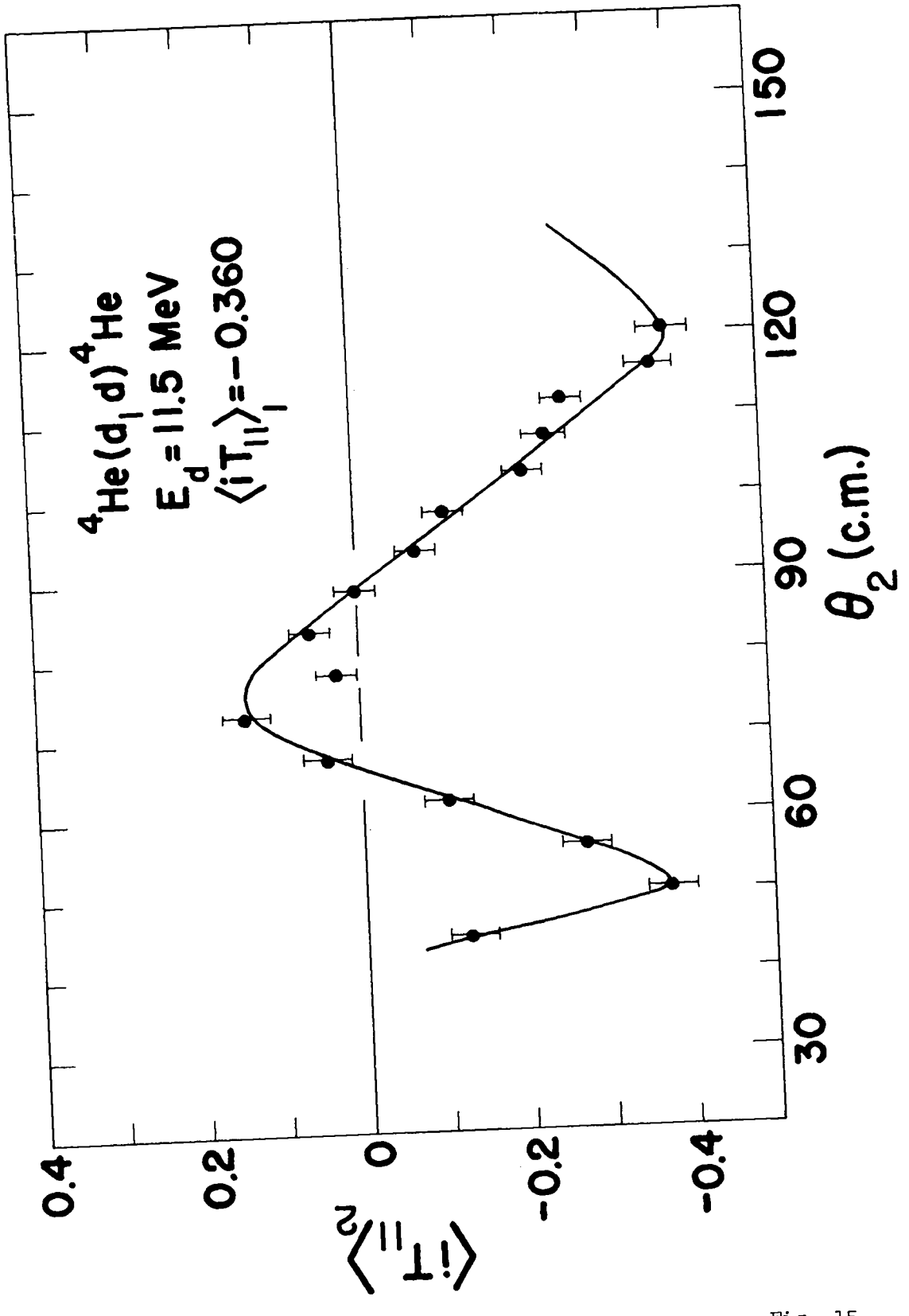
$^4He(d_1,d)^4He$
$E_d = 11.5$ MeV
$\langle iT_{11} \rangle_1 = -0.360$
$\langle iT_{11} \rangle_2$
0.4
0.2
0
-0.2
-0.4
30
60
90
120
150
θ_2 (c.m.)

Fig. 15

is the asymmetry measurement at $\theta_1=\theta_2=118°$ and 11.5-MeV deuteron energy (both scatterings). This measurement may be regarded as the spin-one analogue of the spin-1/2 "P^2 experiment."

From the experimental results illustrated in Fig. 13, the independent ratios $\frac{-(R-L)}{R+L+U+D}$ and $\frac{(R+L)-(U+D)}{R+L+U+D}$ can be formed, where L, U, R, and D represent the total number of counts recorded at azimuthal angles $\phi=0$, 90, 180, and 270°, respectively.

For the measurement taken at a second-scattering angle of 118° (c.m.), we have, from Eqs. (3.1)-(3.3):

$$\frac{b}{a}\Big|_{118°,118°} = \frac{-(R-L)}{R+L+U+D} = \frac{2[\langle iT_{11}\rangle_1\langle iT_{11}\rangle_2-\langle T_{21}\rangle_1\langle T_{21}\rangle_2]}{1+\langle T_{20}\rangle_1\langle T_{20}\rangle_2} \tag{4.1}$$

$$\frac{c}{a}\Big|_{118°,118°} = \frac{(R+L)-(U+D)}{R+L+U+D} = \frac{2[\langle T_{22}\rangle_1\langle T_{22}\rangle_2]}{1+\langle T_{20}\rangle_1\langle T_{20}\rangle_2} . \tag{4.2}$$

From the tensor rotation properties presented in the Appendix, we find:

$$\frac{b}{a}\Big|_{118°,118°} = \frac{2[\langle iT_{11}\rangle\langle iT_{11}\rangle-(0.5077\langle T_{20}\rangle-0.5592\langle T_{21}\rangle+0.4145\langle T_{22}\rangle)\langle T_{21}\rangle]}{1+[-0.1694\langle T_{20}\rangle+1.015\langle T_{21}\rangle+0.9548\langle T_{22}\rangle]\langle T_{20}\rangle} \tag{4.3}$$

$$\frac{c}{a}\Big|_{118°,118°} = \frac{2[0.4774\langle T_{20}\rangle-0.4145\langle T_{21}\rangle+0.6102\langle T_{22}\rangle]\langle T_{22}\rangle}{1+[-0.1694\langle T_{20}\rangle+1.0154\langle T_{21}\rangle+0.9548\langle T_{22}\rangle]\langle T_{20}\rangle} , \tag{4.4}$$

where an appropriate rotation has been made so that the tensor parameters with subscript 1 are referred to a coordinate system whose z-axis coincides with the incoming laboratory direction for the second

scattering ($\vec{k}_{in}$) and whose y-axis coincides with $\vec{k}_{in}\times\vec{k}_{out}$. The parameters with subscript 2 are referred to the outgoing center-of-mass direction for the second scattering.

The values of b/a and c/a for a range of angles are given in Table VI and are shown in Fig. 16. By averaging the three data points nearest θ_2=118°, we find $\frac{b}{a}|_{118°,118°}$=0.260±0.002 and $\frac{c}{a}|_{118°,118°}$= 0.069±0.008.

4.4 Calibration Procedure

For a system possessing axial symmetry about an axis (such as a deuteron beam produced by a polarized-ion source), two non-zero parameters are sufficient to describe the polarization. In terms of the fractional populations $N_\uparrow$ N_o $N_\downarrow$ along the symmetry axis, the tensors characterizing such a beam may be written (Sc 68):

$$\langle t_{10}\rangle = \sqrt{\frac{3}{2}}\,(N_\uparrow - N_\downarrow)$$

$$\langle t_{20}\rangle = \sqrt{\frac{1}{2}}\,(1 - 3N_o)\ .$$

If the polarized beam is scattered from a target with analyzing power described by the tensors $\langle iT_{11}\rangle$, $\langle T_{20}\rangle$, $\langle T_{21}\rangle$, and $\langle T_{22}\rangle$, then the ratios analogous to those measured in the double-scattering experiment can be expressed as:

$$\frac{b}{a} = \frac{D^1_{01}\langle t_{10}\rangle\langle iT_{11}\rangle + D^2_{01}\langle t_{20}\rangle\langle T_{21}\rangle}{1 + D^2_{00}\langle t_{20}\rangle\langle T_{20}\rangle} \qquad (4.5)$$

TABLE VI

RATIOS b/a AND c/a FOR 11.5-MeV DEUTERON ENERGY

E_d(lab) for second scattering (MeV)	θ_2(c.m.)	b/a	c/a
11.5	56.05	0.193±0.021	-0.104±0.016
11.5	61.68	0.075±0.020	-0.026±0.014
11.5	67.22	-0.031±0.021	0.098±0.014
11.5	72.68	-0.100±0.020	0.068±0.014
11.5	78.02	-0.019±0.020	0.096±0.013
11.5	83.26	-0.043±0.019	0.100±0.013
11.5	88.38	-0.001±0.020	0.111±0.013
11.5	93.37	0.054±0.018	0.096±0.012
11.5	98.22	0.078±0.017	0.114±0.012
11.5	102.93	0.150±0.017	0.124±0.011
11.5	107.49	0.168±0.019	0.090±0.013
11.5	111.89	0.183±0.017	0.090±0.012
11.5	116.13	0.245±0.018	0.083±0.012
11.5	118.19	0.244±0.020	0.066±0.014
11.5	120.22	0.264±0.020	0.058±0.014

Figure 16. Values of b/a and c/a extracted from the data of Fig. 13. The solid curve is a theoretical prediction obtained from a phase-shift analysis employing the measured asymmetries of the present experiment.

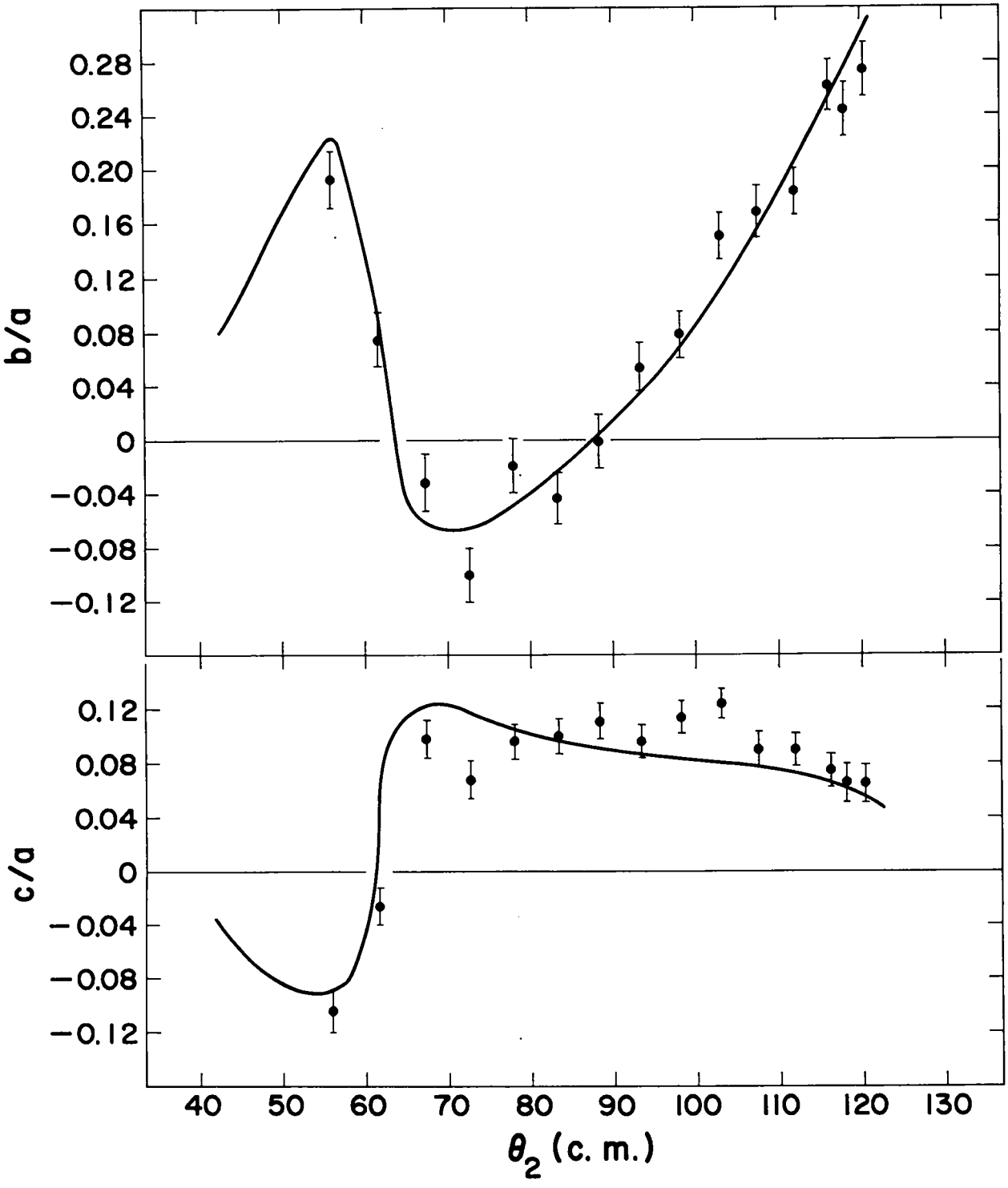
0.28
0.24
0.20
0.16
0.12
0.08
0.04
0
−0.04
−0.08
−0.12
b/a
0.12
0.08
0.04
0
−0.04
−0.08
−0.12
c/a
40
50
60
70
80
90
100
110
120
130
θ2 (c. m.)

Fig. 16

and

$$\frac{c}{a} = \frac{D_{02}^2 \langle t_{20} \rangle \langle T_{22} \rangle}{1 + D_{00}^2 \langle t_{20} \rangle \langle T_{20} \rangle} \quad . \tag{4.6}$$

The $D^K_{Q'Q}$'s are the rotation matrices as defined by Rose (Ro 57), and are functions of the Euler angles which describe the rotation between the original reference frame and a reference frame with z-axis along the incident beam direction for the second scattering and y-axis along $\vec{k}_{in} \times \vec{k}_{out}$ (see Appendix). Equations (4.5) and (4.6) involve six variables. If the $D^K_{Q'Q}$'s are varied (e.g., by changing the magnetic field direction in the polarized source ionizer), and the quantities b/a and c/a are measured for each magnetic field configuration, four linear independent relations can be obtained. Taken together with the relations (4.3) and (4.4), and with the experimental values for $\frac{b}{a}|_{118°,118°}$ and $\frac{c}{a}|_{118°,118°}$ presented in Table VI, six linear inhomogeneous equations are obtained. Thus, all six variables ($\langle t_{10} \rangle$, $\langle t_{20} \rangle$, $\langle iT_{11} \rangle$, $\langle T_{20} \rangle$, $\langle T_{21} \rangle$, $\langle T_{22} \rangle$) may be determined. It is to be understood that the ion source measurements must be done at 118° (c.m.) and 11.5-MeV deuteron energy.

4.5 Summary

This approach does not involve any assumptions as to the relative magnitudes of the various tensor parameters. However, the present work as well as all previous d-^{4}He studies have indicated that 1) the tensor component $\langle T_{21} \rangle$ is small compared to the vector polarization $\langle iT_{11} \rangle$, and 2) the parameter $\langle T_{20} \rangle$ is small compared to one. A

phase-shift analysis based on the asymmetry measurements shown in Fig. 11 in conjunction with other available d-^{4}He cross section and polarization data predicts the following values for the tensor moments: $\langle T_{20}\rangle=0.0500$, $\langle T_{21}\rangle=0.0583$, $\langle T_{22}\rangle=0.1732$, and $\langle iT_{11}\rangle=-0.3745$.* Extensive investigation of the phase-shift solutions shows that $\langle T_{20}\rangle$ and $\langle T_{21}\rangle$ are in any case very small. Thus, in view of the magnitudes of the second-order tensor parameters, the data shown in Fig. 13 may be regarded as primarily useful in the determination of the vector polarization of a deuteron beam.

*These predictions are based on the corrected version of SPINONE.

CHAPTER V

INVESTIGATION OF THE REACTION $^{3}He(d,p)^{4}He$ INDUCED WITH POLARIZED DEUTERONS

5.1 Introduction

Recent experimental advances have made available a wealth of data on the process $^{3}He(d,p)^{4}He$ which presents a considerable challenge to the models of nuclear reaction mechanisms. The proton polarization experiments of Brown et al. (Br 63) together with the asymmetry experiment of Baker et al. (Ba 65) using a polarized ^{3}He target have been shown by Tanifuji (Ta 65) to contradict some basic assumptions of direct interaction models for the process. A satisfactory theoretical description of the $^{3}He(d,p)^{4}He$ reaction (or its mirror reaction $T(d,n)^{4}He$) has not been made, except for very low deuteron energies where the cross sections can be described primarily in terms of a resonance forming ^{5}Li (or ^{5}He) in a state of total angular momentum $J=3/2^{+}$.

The present investigation was undertaken in order to supplement existing elastic scattering and reaction measurements which may be used in a theoretical analysis of the five-nucleon system. The work presented in this chapter is an investigation of the Right-to-Left proton asymmetry in the $^{3}He(d,p)^{4}He$ reaction using a deuteron beam with vector polarization $\langle iT_{11}\rangle=-0.360\pm0.015$ obtained from alpha-deuteron elastic scattering. Asymmetry measurements were made at 15 center-of-mass angles between 20° and 160° for 10.0-, 12.0-, and

14.0-MeV deuterons. The investigation extends the range of similar asymmetry measurements between 6.0 and 10.0 MeV by Plattner (Pl 68) of the University of Wisconsin.

A reaction matrix analysis using the present results as well as previously existing d-^{3}He and p-^{4}He cross sections and polarization data is being employed in an effort to provide a satisfactory theoretical description of the five-nucleon system (Do 68).

5.2 Apparatus

5.2a General Arrangement

A cross-sectional view of the experimental apparatus is shown in Fig. 17. As in the deuteron polarization measurements, the first target contained deuterium gas at liquid-nitrogen temperatures, and was bombarded by alpha particles from the LAVEC. The second gas target, located at the center of the second-scattering chamber, contained ^{3}He gas, in which the polarized deuterons induced the ^{3}He(d,p)^{4}He reaction. The second-scattering chamber was evacuated and the cell was pressurized to 10.0 atmospheres (absolute) with ^{3}He gas. The reaction protons were detected by two counter telescopes, each of which consisted of a 500-μm thick surface barrier detector located behind a 300-μm thick totally depleted ΔE detector (see Fig. 5).

5.2b The ^{3}He Gas Target

The ^{3}He gas target assembly was machined from a stainless steel cylinder and is shown in Fig. 18. Helium-3 gas of 96% purity was contained within a 1.000-inch diameter region which was 1.000 inch

Figure 17. Basic experimental apparatus used in the study of the reaction $^{3}He(d,p)^{4}He$. Indicated are the high-pressure gas cell and fixed collimation system which permitted the cell and detector assemblies to be rotated about the beam axis. (The figure is not drawn to scale.)

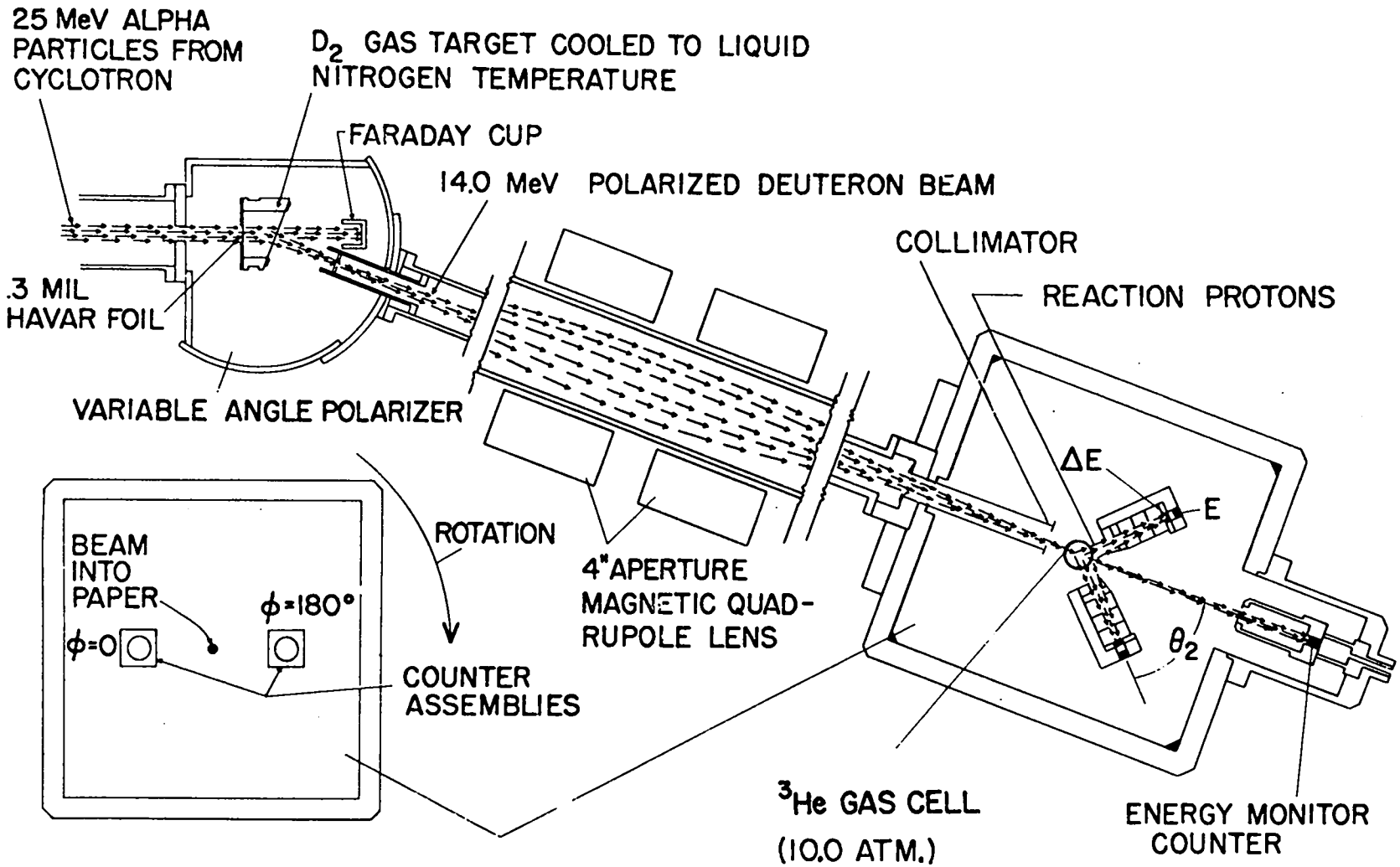

CROSS SECTION TARGET CHAMBER

Fig. 17

Figure 18. ^{3}He gas-target assembly showing the gas inlet, confinement region, stainless steel posts, and supporting arms. The 0.0005-in. thick Havar foil is not indicated.

^{3}He GAS TARGET ASSEMBLY

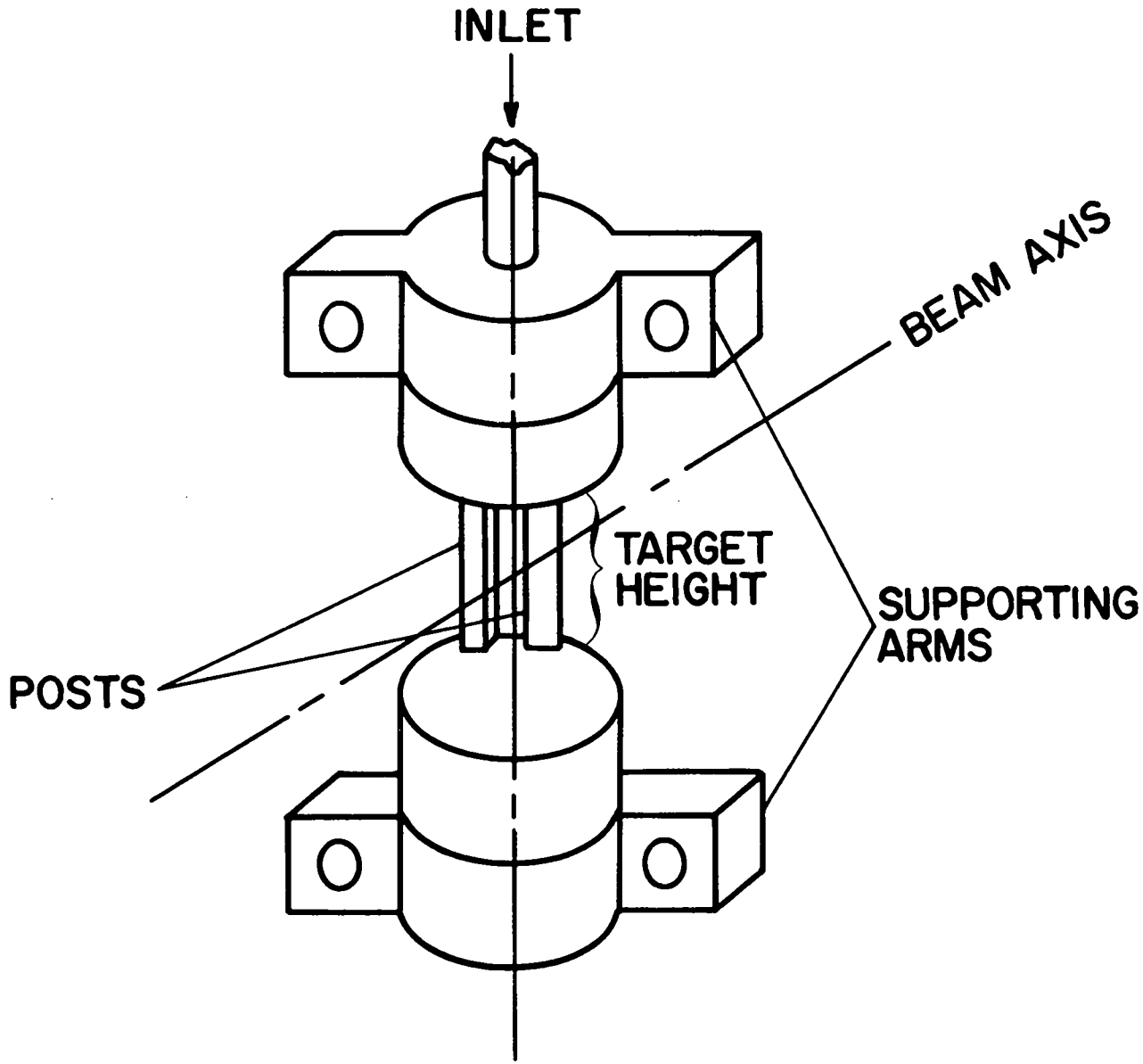

Fig. 18

long. Except for two posts positioned 0.375 inches apart, the walls of the cylinder consisted of 0.0005-inch thick Havar foil attached with epoxy resin.* In assembling the gas cell, the Havar foil was wrapped around the entire portion of the assembly between the supporting arms and was glued in place. The whole assembly was then heated in an oven to cure the adhesive.

The ^{3}He gas cell was quite hardy and could withstand a pressure of 15 atmospheres. The size of the windows could have been reduced slightly; however, the cell was sufficiently rigid, and, more importantly, no failure ever occurred after the cell had been successfully pressurized.

The gas target was firmly supported by means of rods which passed from the rear of the second-scattering chamber through the holes in the supporting arms. This arrangement allowed the detector slit assemblies free movement while being positioned to within 0.25 inch of the target cell. Since the cell was free to rotate about the beam axis, the geometry of the two detector assemblies with respect to the gas cell remained fixed for any second-scattering angle.

5.2c Beam Collimation

Collimation of the deuteron beam was accomplished by requiring the beam to pass through a 0.50-inch by 0.25-inch rectangular aperture located 1.0 inch from the center of the ^{3}He cell. This small aperture was desirable in order to improve the energy resolution of the system

---

*Armstrong A-6 with Activator E, supplied by Armstrong Products, Warsaw, Illinois.

(over that used in the d-^{4}He double-scattering measurements) and to prevent the posts of the ^{3}He gas cell from interfering with the deuteron beam. For angles greater than 140° (c.m.), the collimator and absorber foils were withdrawn to 2.0 inches from the gas cell in order to allow the detector assemblies to reach the far back angles. Because of the small collimator aperture, the extreme angular acceptance of the scattered deuterons from the first target into the ^{3}He cell was ±3° (c.m.) from the mean scattering angle in the horizontal plane.

5.2d Absorber Foils and Detector Slit Assemblies

Absorber foils to adjust the energy of the polarized deuteron beam were positioned immediately adjacent to the rectangular collimator. This position was chosen in order to reduce angular spreading of the deuteron beam as much as possible without interfering with the path of the reaction protons. By using aluminum absorber foils of 0.0133 inch and 0.0072 inch in thickness, the energy of the polarized beam could be adjusted to 10.0 and 12.0 MeV, respectively. No absorber foil was required for the asymmetry measurement at 14.0-MeV deuteron energy.

For the various deuteron energies, the reaction protons emerging from the gas target varied in energy from 10 MeV to 30 MeV over the observed angular range. Thus, to prevent unwanted coincidence events, the detector slit assemblies used in the d-^{4}He polarization measurements were replaced with similar slits made of 0.062-inch thick tantalum.

5.3 Experimental Procedure

5.3a Alignment of the System

At deuteron energies near 10.0 MeV, the $^{3}He(d,p)^{4}He$ reaction cross section varies quite rapidly at small center-of-mass angles (St 60). Thus, very small alignment errors or deviations of the beam from the axis of the system could result in significant errors in the measured Right-to-Left intensity ratios. To reduce these sources of error, considerable care was exercised in properly collimating the deuteron beam and in aligning the system.

In order to provide measurements over the largest possible angular range, the ^{3}He gas cell was designed to be used in the "posts upstream" position for second-scattering angles below 90° (lab) and to be positioned in the "posts downstream" configuration for angles larger than 90° (lab). A 0.50-inch by 0.25-inch rectangular collimator was positioned 1.0 inch from the center of the ^{3}He cell in order to insure that the posts of the cell would not significantly interfere with the bombarding deuteron beam.

The alignment of the beam collimation system and scattering chamber was accomplished as follows. With the collimator in place, a 0.5-mg/cm^{2} gold foil was positioned at the center of the second-scattering chamber. Right-to-Left intensity ratios of elastically-scattered deuterons were then measured for a range of second-scattering angles in order to determine the optimum chamber alignment in the horizontal plane. The gold foil was then removed, and nuclear emulsions positioned at the center of the second-scattering chamber were exposed in order to provide a means of proper beam positioning.

The ^{3}He gas cell was then mounted at the center of the chamber and measurements of the reaction proton yield at 90° (lab) were made for the cell in both of its configurations. For a 90° (lab) measurement, the detector slit assemblies defined a target within the ^{3}He cell such that the posts of the cell did not interfere with the observed solid angles. This geometry made it possible to compare measurements with the gas cell both in the "posts upstream" and "posts downstream" position to detect false asymmetries in the proton yield. Statistically consistent results indicated that the ^{3}He cell could be oriented in the desired positions for measuring both forward and backward angles without introducing any systematic error.

5.3b Proton Asymmetry Measurements

The polarized deuteron beam was obtained from deuteron-alpha elastic scattering at 11.5-MeV equivalent deuteron energy. The vector polarization of the deuterons recoiling at 118° (c.m.) was $\langle iT_{11} \rangle = 0.360 \pm 0.015$ or 42% of its maximum possible value. The 14.0-MeV recoiling deuterons were then passed through a magnetic quadrupole focusing lens and collimated by a 0.25×0.50-inch rectangular collimator. After collimation, the beam was slowed with aluminum foil before entering the ^{3}He cell. The polarized beam had an intensity of ∿5 pa and an energy spread of ±300 keV. This intensity was sufficient to yield and average of about 100 counts/hr in the two detectors.

As in the d-^{4}He polarization measurements, the effects of fluctuations in the beam intensity were eliminated by rotating the chamber about the beam axis and determining the geometric mean of the

Right-to-Left counting ratios. Besides eliminating the effects of possibly inaccurate current integration, this procedure avoided errors caused by small differences in the counter efficiencies and second-scattering angles. In all cases, the detector slit systems provided an angular resolution of ±2.5° in the center-of-mass system.

The scattering chamber was designed so that for a given second-scattering angle (θ_2) four telescopes could be mounted at azimuthal angles (ϕ_2) of 0, 90, 180, and 270°. In the present experiment, only two telescopes were used. These were set at ϕ_2=0° and 180° corresponding to Left and Right, respectively. Thus, a measurement at a particular angle θ_2 consisted of two runs, with the chamber rotated through 180° after each run.

The reaction products were detected by two E-ΔE detector telescopes employing silicon surface-barrier detectors. A coincidence requirement between the corresponding ΔE and E detectors reduced the background to a negligible amount. The ΔE and E pulses along with the telescope designation were recorded event by event on magnetic tape with a 4096-channel two-dimensional analyzer acting as a buffer. The magnetic tape was processed off-line to produce two-dimensional ΔE vs E plots and tables for each telescope.

5.3c Background Measurements

Background measurements were made by replacing the ^{3}He gas cell by an identical evacuated cell. The largest source of possible background events was due to (d,p) reactions in the Havar foil of the gas target. In addition, (d,p) reactions could also occur in the

aluminum and tantalum parts of the slit assemblies. However, there was little difficulty in distinguishing these background protons from the more energetic $^{3}He(d,p)^{4}He$ reaction protons. By placing absorber foils both between the detectors and in front of the ΔE counter and imposing coincidence conditions, it was possible to eliminate the effects due to background. The absorber foil between the detectors was also instrumental in stopping alpha particles from (n,α) reactions within the silicon detectors. (This latter effect was the major source of background encountered during the course of the d-^{4}He polarization measurements.) The practice of taking background runs was continued throughout the course of the experiment to insure that spurious pulses were not being generated in the electronic system.

5.4 Experimental Results

The vector analyzing power $\langle iT_{11}\rangle_2$ of the reaction can be expressed in terms of the Right-to-Left scattering ratio by the following relation:

$$\frac{R}{L} = \frac{1 - 2\langle iT_{11}\rangle_1\langle iT_{11}\rangle_2}{1 + 2\langle iT_{11}\rangle_1\langle iT_{11}\rangle_2} \quad , \tag{5.1}$$

where $\langle iT_{11}\rangle_1 = -0.360 \pm 0.015$ as determined by the d-^{4}He polarization results (see Chapter IV). In writing Eq. (5.1), terms resulting from second-rank polarization have been neglected. Rewriting:

$$\langle iT_{11}\rangle_2 = \frac{1}{2(-0.360)} \left(\frac{L-R}{L+R}\right) \quad ,$$

where L and R represent geometric mean values.

The measured values of $\langle iT_{11} \rangle_2$ for 10.0-, 12.0-, and 14.0-MeV deuteron energy over a range of second-scattering angles are presented in Table VII and Figs. 19-21. The majority of the data points represent average values of two measurements. The data displays the following general characteristics. For all three deuteron bombarding energies, the moment $\langle iT_{11} \rangle_2$ exhibits large negative values in the region of 40° (c.m.) and large positive values in the region of 120° (c.m.). In addition, there exists at each energy a relatively constant negative polarization over the angular range 50°-70° (c.m.).

Figure 19 illustrates the values of $\langle iT_{11} \rangle_2$ obtained at 10.0-MeV deuteron energy from the present experiment together with the results of Plattner (Pl 68). With the exception of the angular range 120°-150° (c.m.), the results appear to be in excellent agreement. Figures 20 and 21 illustrate the values of $\langle iT_{11} \rangle_2$ for 12.0- and 14.0-MeV deuteron energy, respectively. The largest asymmetry measured was at 10.0 MeV, 121° (c.m.), where R/L=3.47±0.27. In all cases, $\langle iT_{11} \rangle_2$ approaches zero at θ_2=0°, 180° (c.m.) as expected on the basis of the characteristics of the spin-orbit nuclear force. The errors expressed in Figs. 19-21 and Table VII are statistical errors only.

5.5 Accuracy of the Measurements

The results of extensive phase analysis of the present d-^{4}He polarization measurements in conjunction with previously existing cross section data has consistently indicated that the spin tensor moment $\langle T_{21} \rangle$ is small compared to the moment $\langle iT_{11} \rangle$ in the region

TABLE VII

REACTION VECTOR POLARIZATION AT 10.0-, 12.0-, AND 14.0-MeV DEUTERON ENERGY

E_d(lab) (MeV)	θ_2(c.m.)	$\langle iT_{11} \rangle_2$	E_d(lab) (MeV)	θ_2(c.m.)	$\langle iT_{11} \rangle_2$	E_d(lab) (MeV)	θ_2(c.m.)	$\langle iT_{11} \rangle_2$
10.0	19.21	-0.195±0.031	12.0	19.43	-0.257±0.028	14.0	19.62	-0.190±0.027
10.0	23.98	-0.325±0.031	12.0	24.26	-0.441±0.027	14.0	24.49	-0.402±0.030
10.0	30.00	-0.535±0.031	12.0	36.23	-0.701±0.029	14.0	36.58	-0.603±0.034
10.0	35.82	-0.614±0.035	12.0	42.15	-0.570±0.033	14.0	42.55	-0.407±0.026
10.0	41.69	-0.653±0.035	12.0	48.02	-0.313±0.028	14.0	48.47	-0.192±0.027
10.0	47.50	-0.549±0.031	12.0	59.57	-0.165±0.025	14.0	60.11	-0.068±0.023
10.0	53.26	-0.336±0.031	12.0	70.84	-0.126±0.025	14.0	71.45	0.017±0.026
10.0	58.95	-0.199±0.031	12.0	81.77	-0.090±0.030	14.0	82.43	0.029±0.034
10.0	70.12	-0.149±0.031	12.0	92.34	0.099±0.036	14.0	93.04	0.264±0.039
10.0	81.00	-0.121±0.031	12.0	102.50	0.431±0.037	14.0	103.25	0.600±0.035
10.0	91.53	0.031±0.031	12.0	112.34	0.726±0.037	14.0	113.04	0.660±0.037
10.0	101.73	0.398±0.041	12.0	121.77	0.709±0.037	14.0	122.43	0.609±0.033
10.0	111.53	0.570±0.039	12.0	132.61	0.532±0.037	14.0	132.33	0.560±0.040
10.0	121.00	0.767±0.045	12.0	145.51	0.460±0.032	14.0	145.16	0.398±0.030
10.0	130.12	0.756±0.041	12.0	158.65	0.138±0.035	14.0	158.98	0.132±0.028
10.0	142.40	0.592±0.036						
10.0	150.85	0.428±0.031						
10.0	158.29	0.225±0.031						

Figure 19. Comparison of present vector polarization measurements with those of Plattner (Pl 68), which were obtained with a polarized-ion source. Both experiments were conducted at 10.0-MeV equivalent deuteron energies.

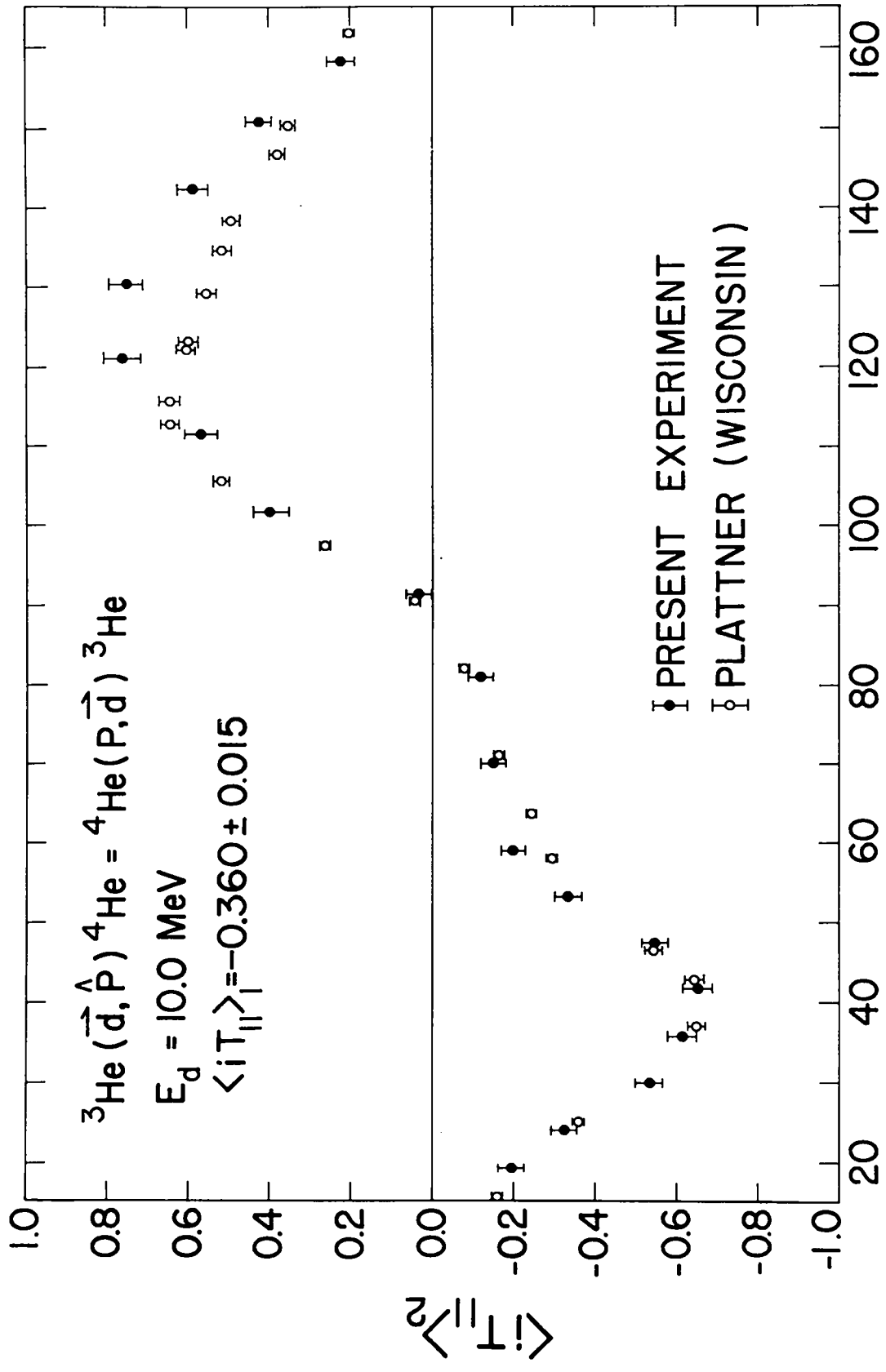
$^3He(\vec{d},\hat{P})^4He = {}^4He(P,\vec{d})^3He$
E_d = 10.0 MeV
$\langle iT_{11}\rangle$=−0.360 ± 0.015
PRESENT EXPERIMENT
PLATTNER (WISCONSIN)
θ_2 (c.m.)
$\langle iT_{11}\rangle_2$
1.0
0.8
0.6
0.4
0.2
0.0
-0.2
-0.4
-0.6
-0.8
-1.0
20
40
60
80
100
120
140
160

Fig. 19

Figure 20. Vector polarization measurements from the $^{3}He(d,p)^{4}He$ reaction at 12.0-MeV deuteron energy.

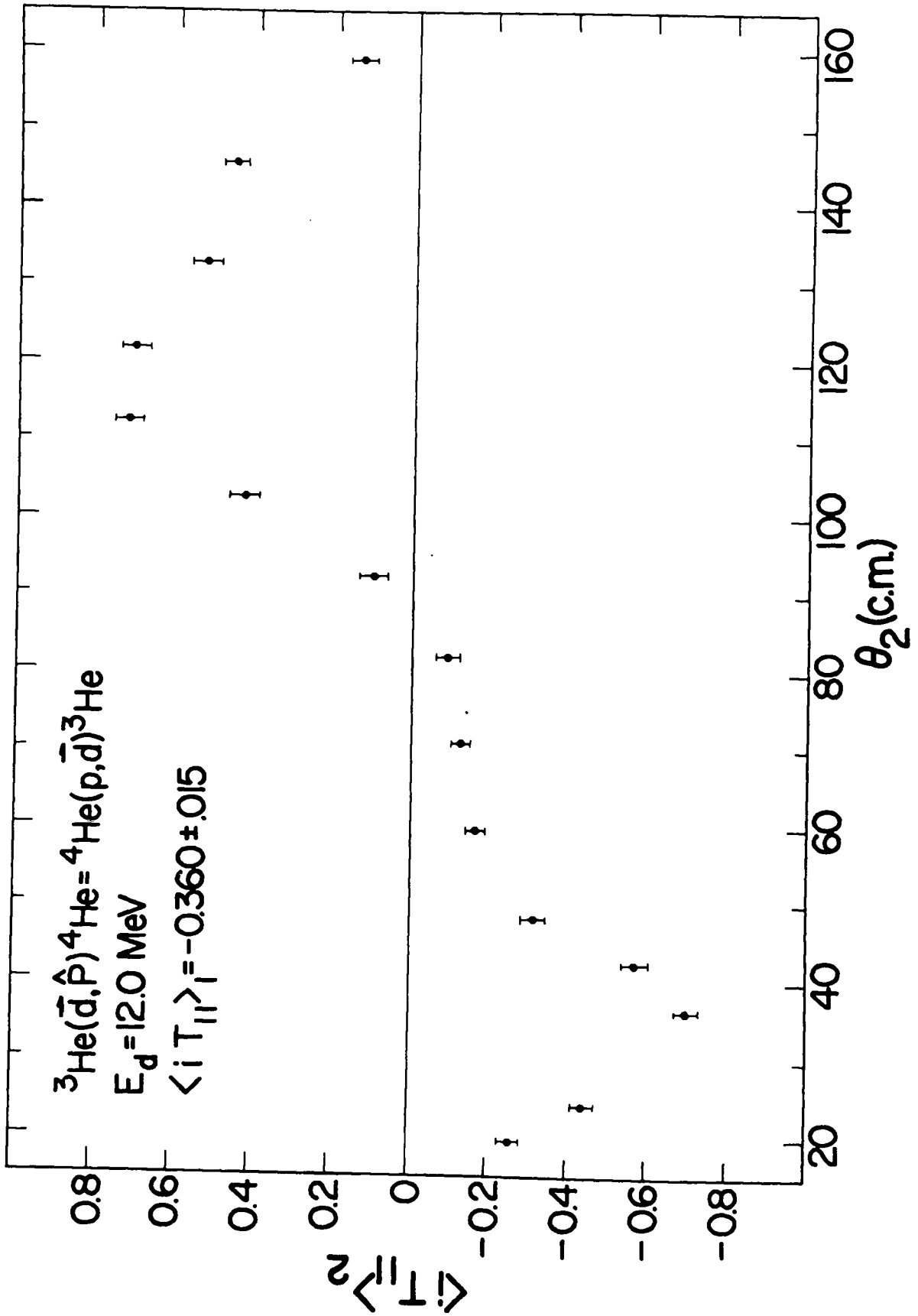
$^3He(\vec{d},\hat{P})^4He = ^4He(p,\vec{d})^3He$
$E_d = 12.0$ MeV
$\langle i T_{11} \rangle = -0.360 \pm .015$
$\langle iT_{11} \rangle_2$
θ_2(c.m.)
0.8
0.6
0.4
0.2
0
-0.2
-0.4
-0.6
-0.8
20
40
60
80
100
120
140
160

Fig. 20

Figure 21. Vector polarization measurements from the $^{3}He(d,p)^{4}He$ reaction at 14.0-MeV deuteron energy.

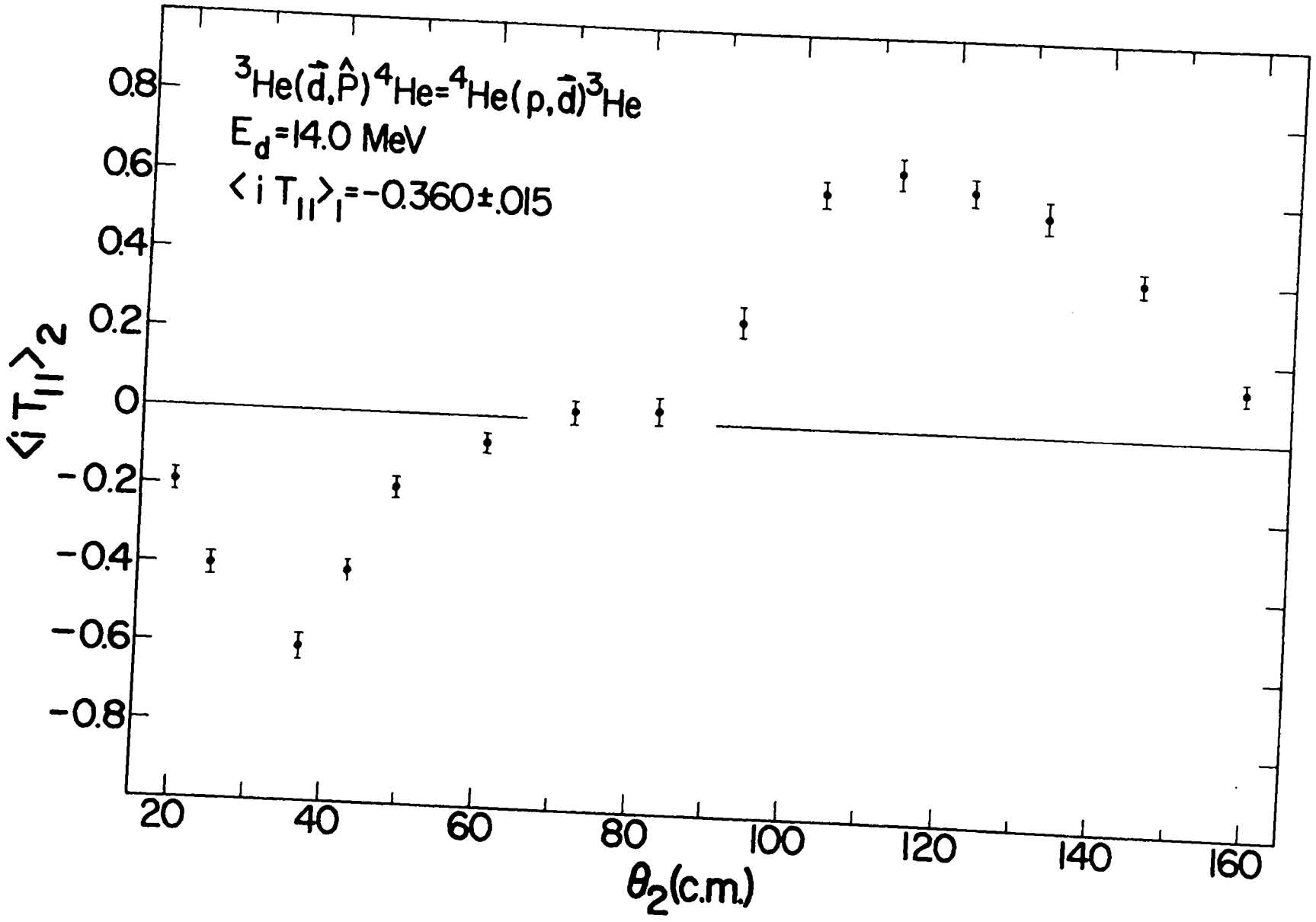
$^3He(\vec{d},\hat{P})^4He = {}^4He(p,\vec{d})^3He$
E_d=14.0 MeV
$\langle i T_{11} \rangle_1$=-0.360±.015
$\langle i T_{11} \rangle_2$
0.8
0.6
0.4
0.2
0
-0.2
-0.4
-0.6
-0.8
20
40
60
80
100
120
140
160
θ_2(c.m.)

Fig. 21

of 118° (c.m.). Either moment is capable of producing a Right-to-Left asymmetry in the reaction proton yield. Although it is possible to separate these parameters by using magnetic fields between the scatterings to rotate the spin of the intermediate beam (Bu 60), this method was not feasible under the present circumstances. Thus, the effect of tensor polarization resulting from the first scattering was neglected in the presentation of the results. In actual fact, the moment $\langle T_{21} \rangle$ has a predicted value at $\theta_1=118°$ (c.m.) of $\langle T_{21} \rangle=0.050$. An uncertainty in the vector polarization of the deuteron beam as large as 5% could result from this tensor polarization effect. Such an uncertainty could introduce an error as large as 0.025 in the value of $\langle iT_{11} \rangle_2$.

An effect of the finite ^{3}He target is the possibility of false asymmetries caused by the energy and intensity variation of the incident deuterons across the entrance to the gas cell. These variations are caused by the spread in energy loss in the first scattering and the variation of the d-^{4}He elastic cross section within the angular acceptance interval of the ^{3}He cell. In order to obtain an estimate of the maximum error introduced into the results, the center of mass of the deuteron beam was assumed to be off center by 25% of the target width in the scattering plane. Even for this extreme case, no errors larger than 0.013 would be introduced into the value of $\langle iT_{11} \rangle_2$.

Statistical uncertainties in the values of $\langle iT_{11} \rangle_2$ as presented in Table VII ranged from 0.023 to 0.045, with 0.032 being the average statistical uncertainty. The stated results for forward angles (less

than 30° (c.m.)), and over the region 90°-140° (c.m.) are averages of two independent measurements.

The energy resolution of the polarized deuteron beam after collimation (±300 keV) was considerably better than that employed in the d-^{4}He polarization measurements. The more restrictive collimation system used in the present experiment was assumed to not affect the vector polarization of the beam ($\langle iT_{11} \rangle_1$=-0.360±0.015).

The results of nuclear emulsion exposures indicated that very little profile distortion of the beam had occurred after the collimator and absorber foils were withdrawn to 2.0 inches from the center of the ^{3}He gas cell. Consequently, no correction was applied to back angle measurements because of this procedure.

Although the ^{3}He gas used in this experiment contained an impurity of approximately 4% ^{4}He, no correction was necessary because of the gas impurity. Elastically scattered deuterons from both the Havar foils and the ^{4}He gas were prevented from penetrating the ΔE-E detector system by absorber foils placed in front of the ΔE detectors and between the E and ΔE detectors. Protons from (d,p) reactions within the absorber foils, target foils, and detector slit systems were similarly prevented from penetrating the detector system.

Measurements of the proton yield taken at the start and near the end of the experiment indicated no significant loss of pressure in the ^{3}He gas cell occurred during the course of the experiments.

In summary, the present results at 10.0-MeV deuteron energy appear to be in agreement, within statistics, with the measurements

of Plattner (Pl 68), if possible tensor polarization effects are taken into consideration.

5.6 Discussion

The expression $^{3}He(\vec{d},\hat{p})^{4}He = {}^{4}He(p,\vec{d})^{3}He$ in Figs. 19-21 is to indicate that no new additional information can be obtained by bombarding ^{4}He nuclei with unpolarized protons and measuring the resultant deuteron polarization. The relationship between the two experiments can be illustrated as follows: The expression $^{3}He(\vec{d},\hat{p})^{4}He$ represents a reaction in which polarized deuterons are incident on an unpolarized ^{3}He target, and a proton asymmetry (represented by the hat ^) is determined.

The Right-to-Left proton scattering ratio can be expressed in terms of the vector analyzing power of the reaction as follows:

$$\frac{R}{L} = \frac{1 - 2\langle iT_{11}\rangle_1 \langle iT_{11}\rangle_2}{1 + 2\langle iT_{11}\rangle_1 \langle iT_{11}\rangle_2} \quad , \tag{5.2}$$

where the tensor parameters of the deuteron beam are assumed to be zero. Thus, the vector analyzing power of the reaction is proportional to the proton asymmetry. If the reaction were to be run backwards in time, a deuteron polarization of the opposite sign (but same magnitude) would result because of the effect of the spin-orbit force expressed by the term $\langle iT_{11}\rangle_2$. The center-of-mass energy equivalent to 14.0-MeV deuterons incident on ^{3}He, for example, is 33.4-MeV protons incident on ^{4}He. Thus, the experiment $^{4}He(p,\vec{d})^{3}He$ does not provide any additional information over that which can be

obtained from a study of the reaction $^{3}He(\vec{d},\hat{p})^{4}He$. The former experiment, of course, would require a known deuteron polarization analyzer in order to determine the deuteron polarization resulting from the reaction. This consequence of time-reversal invariance is a generalization of the polarization-asymmetry theorem for spin-1/2 particles which states that the azimuthal asymmetry in the outgoing beam for a reaction with polarized incident beam is equal to the polarization produced in the inverse reaction with unpolarized incident beam (Bl 51, Sa 58, Bi 59).

Table VIII presents the non-equivalent cross section and polarization experiments which could be performed for the mass-five system.

TABLE VIII

FIVE-NUCLEON PROBLEMS

3(2,2)3	3(2,1)4⇆4(1,2)3	4(1,1)4
a. 3(2,2)3	j. 3(2,1)4	r. 4(1,1)4
b. 3(2,$\vec{2}$)3	k. 3(2,$\vec{1}$)4	s. 4(1,$\vec{1}$)4
c. 3($\vec{2}$,$\vec{2}$)3	l. 3($\vec{2}$,$\hat{1}$)4	t. 4($\vec{1}$,$\vec{1}$)4
d. 3(2,2)$\vec{3}$	m. 3($\vec{2}$,$\vec{1}$)4	
e. $\vec{3}$(2,2)$\vec{3}$	n. $\vec{3}$(2,$\hat{1}$)4	
f. 3($\vec{2}$,2)$\vec{3}$	o. $\vec{3}$(2,$\vec{1}$)4	
g. $\vec{3}$($\vec{2}$,$\vec{2}$)3	p. $\vec{3}$($\vec{2}$,$\hat{1}$)4	
h. $\vec{3}$($\vec{2}$,2)$\vec{3}$	q. $\vec{3}$($\vec{2}$,$\vec{1}$)4	
i. $\vec{3}$($\vec{2}$,$\hat{2}$)$\hat{3}$		

The arrows (→) above the atomic mass numbers indicate polarization, while the hats (^) indicate that an asymmetry is to be measured. Each experiment is capable of providing new information on the $^{3}He(d,p)^{4}He$ and $T(d,n)^{4}He$ reactions (Ke 68). The reactions or elastic scatterings without either arrows or hats indicate unpolarized cross section measurements. The experiment presented in the present chapter corresponds to experiment 1, where 3=^{3}He, 2=d, 1=p, and 4=^{4}He. As mentioned previously, this approach also applies to the $T(d,n)^{4}He$ reaction. Although the arrows do not distinguish between vector and tensor polarization, experiments which use beams of tensor polarized deuterons ($\langle T_{20} \rangle$, $\langle T_{21} \rangle$, $\langle T_{22} \rangle$) will undoubtedly be necessary in order to completely describe the five-nucleon system. Thus, a total of 74 independent experiments could be performed involving the d-^{3}He and p-^{4}He channels at a particular equivalent center-of-mass energy.

APPENDIX

ROTATION PROPERTIES OF THE SPIN TENSOR MOMENTS

The spin tensor moments $\langle T_{KQ} \rangle$ transform under a rotation of the coordinate system C in C' through the Euler angles $(\alpha\beta\gamma)$ according to the relation:

$$\langle T_{KQ}(C') \rangle = \sum_{Q'} \langle T_{KQ'}(C) \rangle \, D^{K}_{Q'Q}(\alpha\beta\gamma), \tag{1}$$

(Sa 60).

The $D^{K}_{Q'Q}(\alpha\beta\gamma)$ are the elements of the rotation matrix $R=e^{-i\alpha S_Z} e^{-i\beta S_Y} e^{-i\gamma S_Z}$, where the S_i's are the components of the spin operator (Ro 57, Eq. 4.7). The factored dependence of the $D^{K}_{Q'Q}(\alpha\beta\gamma)$ on the Euler angles becomes:

$$D^{K}_{Q'Q}(\alpha\beta\gamma) = e^{-i\alpha Q'} \, d^{K}_{Q'Q}(\beta) \, e^{-i\gamma Q} , \tag{2}$$

since we are dealing with representations in which the matrices of S_Z are diagonal. The $d^{K}_{Q'Q}(\beta)$ are referred to as reduced rotation matrices.

The rotation matrix for a first-rank tensor operator can be determined in a straightforward manner by expanding the quantity $e^{-i\beta S_Y}$ which gives:

$$e^{-i\beta S_y} = 1 - i\beta S_Y - S_Y^2 \frac{\beta^2}{2!} + iS_Y^3 \frac{\beta^3}{3!} + S_Y^4 \frac{\beta^4}{4!} - \cdots ,$$

where $S_Y = \sqrt{\frac{1}{2}}\begin{pmatrix} o & -i & o \\ i & o & -i \\ o & i & o \end{pmatrix}$. Using the identities $S_Y^4=S_Y^2$ and $S_Y^3=S_Y$ and the expansions

$$\cos x = 1 - \frac{x^2}{2!} + \frac{x^4}{4!} - \cdots ,$$

and

$$\sin x = x - \frac{x^3}{3!} + \frac{x^5}{5!} - \cdots ,$$

the $D^1_{Q'Q}(\beta)$ become:

$$D^1_{Q'Q}(\beta) = S_Y^2[\cos(\beta) - 1] - iS_Y \sin(\beta) + 1 . \qquad (3)$$

From Eqs. (2) and (3) the complete rotation matrix for a first-rank tensor operator then becomes:

$$D^1_{Q'Q}(\alpha\beta\gamma) = \begin{bmatrix} e^{-i\alpha}(\cos^2\frac{\beta}{2})e^{-i\gamma} & -e^{-i\alpha}(\sqrt{\tfrac{1}{2}}\sin\beta) & e^{-i\alpha}(\sin^2\frac{\beta}{2})e^{i\gamma} \\ (\sqrt{\tfrac{1}{2}}\sin\beta)e^{-i\gamma} & \cos\beta & -(\sqrt{\tfrac{1}{2}}\sin\beta)e^{i\gamma} \\ e^{i\alpha}(\sin^2\frac{\beta}{2})e^{-i\gamma} & e^{i\alpha}(\sqrt{\tfrac{1}{2}}\sin\beta) & e^{i\alpha}(\cos^2\frac{\beta}{2})e^{i\gamma} \end{bmatrix} \qquad (4)$$

where the successive lines correspond to Q'=1, 0, -1, and the columns are arranged in the same order from left to right. The reduced matrix elements for a first-rank tensor operator are:

$$d^1_{00}(\beta) = \cos\beta$$

$$d^1_{10} = d^1_{0-1} = -d^1_{-10} = -d^1_{01} = -\sqrt{\tfrac{1}{2}}\sin\beta$$

$$d^1_{11} = d^1_{-1-1} = \cos^2\left(\frac{\beta}{2}\right)$$

$$d^1_{1-1} = d^1_{-11} = \sin^2\left(\frac{\beta}{2}\right) .$$

The tensor product operation of two matrices may be employed to determine the reduced matrix elements for the second-rank tensor operator from the first-rank elements. Reduction of the tensor product yields the composition formula (Me 62, Eq. C.70):

$$d^K_{Q'Q}(\beta) = \sum_{Q'_1,Q_1=-K_1}^{+K_1} \sum_{Q'_2,Q_2=-K_2}^{+K_2} \langle K_1K_2Q'_1Q'_2|KQ'\rangle d^{K_1}_{Q'_1Q_1} d^{K_2}_{Q'_2Q_2} \langle K_1K_2Q_1Q_2|KQ\rangle , \tag{5}$$

For the present case:

$$K_1=K_2=1, \quad K=2, \quad Q',Q=-2, -1, 0, 1, 2.$$

By employing the symmetry relations

$$d^K_{Q'Q} = (-1)^{Q-Q'} d^K_{-Q'-Q} = (-1)^{Q-Q'} d^K_{QQ'} , \tag{6}$$

it is sufficient to determine only nine elements. From Eq. (5) and Table IX:

$$d^2_{00} = \frac{1}{6} d^1_{-1-1}d^1_{11} + \sqrt{\frac{1}{6}}\sqrt{\frac{2}{3}} d^1_{-10}d^1_{10} + \frac{1}{6} d^1_{-11}d^1_{1-1}$$

$$+ \sqrt{\frac{2}{3}}\sqrt{\frac{1}{6}} d^1_{0-1}d^1_{01} + \frac{1}{6} d^1_{00}d^1_{00} + \sqrt{\frac{2}{3}}\sqrt{\frac{1}{6}} d^1_{01}d^1_{0-1}$$

$$+ \frac{1}{6} d^1_{1-1}d^1_{-11} + \sqrt{\frac{1}{6}}\sqrt{\frac{2}{3}} d^1_{10}d^1_{-10} + \frac{1}{6} d^1_{11}d^1_{-1-1} = \frac{1}{2}(3\cos^2\beta - 1)$$

TABLE IX

CLEBSCH-GORDAN COEFFICIENTS AND SPHERICAL HARMONICS

Note: A $\sqrt{\ }$ is to be understood over every coefficient, e.g., for -8/15 read $-\sqrt{8/15}$

Notation:

K	K	...
Q	Q	...

Q_1	Q_2	Coefficients $\langle Q_1 Q_2 \vert KQ \rangle$
Q_1	Q_2	
.	.	
.	.	
.	.	

$Y_1^0 = \sqrt{\frac{3}{4\pi}}\cos\theta$

$Y_1^1 = -\sqrt{\frac{3}{8\pi}}\sin\theta\, e^{i\phi}$

$Y_2^0 = \sqrt{\frac{5}{4\pi}}\left(\frac{3}{2}\cos^2\theta - \frac{1}{2}\right)$

$Y_2^1 = -\sqrt{\frac{15}{8\pi}}\sin\theta\cos\theta\, e^{i\phi}$

$Y_2^2 = \frac{1}{4}\sqrt{\frac{15}{2\pi}}\sin^2\theta\, e^{2i\phi}$

1/2 × 1/2

	1	+1
+1/2 +1/2	1	1 0 / 0 0

			1
+1/2 −1/2	1/2 1/2		
−1/2 +1/2	1/2 −1/2		−1
	−1/2 −1/2		1

1 × 1/2

	3/2	+3/2
+1 +1/2	1	3/2 1/2 / +1/2 +1/2

			3/2 1/2
+1 −1/2	1/3 2/3		
0 +1/2	2/3 −1/3		−1/2 −1/2
	0 −1/2	2/3 1/3	3/2
	−1 +1/2	1/3 −2/3	−3/2
		−1 −1/2	1

2 × 1

	3	+3
+2 +1	1	3 2 / +2 +2

			3 2 1
+2 0	1/3 2/3		
+1 +1	2/3 −1/3		+1 +1 +1
	+2 −1	1/15 1/3	3/5
	+1 0	8/15 1/6	−3/10
	0 +1	6/15 −1/2	1/10

1 × 1

	2	+2
+1 +1	1	2 1 / +1 +1

			2 1 0
+1 −0	1/2 1/2		
0 +1	1/2 −1/2		0 0 0
	+1 −1	1/6 1/2	1/3
	0 0	2/3 0	−1/3
	−1 +1	1/6 −1/2	1/3

			2 1
+1 −1	1/5 1/2		3/10
0 0	3/5 0		−2/5
−1 +1	1/5 −1/2		3/10

			2 1
0 −1	1/2 1/2		2
−1 0	1/2 −1/2		−2
	−1 −1		1

3/2 × 1

	5/2	+5/2
+3/2 +1	1	5/2 3/2 / +3/2 +3/2

			5/2 3/2 1/2
+3/2 0	2/5 3/5		
+1/2 +1	3/5 −2/5		+1/2 +1/2 +1/2
	+3/2 −1	1/10 2/5	1/2
	+1/2 0	3/5 1/15	−1/3
	−1/2 +1	3/10 −8/15	1/6

			3 2 1
0 −1	6/15 1/2		1/10
−1 0	8/15 −1/6		−3/10
−2 +1	1/15 −1/3		3/5

			3 2
−1 −1	2/3 1/3		3
−2 0	1/3 −2/3		−3
	−2 −1		1

2 × 1/2

	5/2	+5/2
+2 1/2	1	5/2 3/2 / 3/2 +3/2

			5/2 3/2
+2 −1/2	1/5 4/5		
+1 +1/2	4/5 −1/5		+1/2 +1/2
	+1 −1/2	2/5 3/5	
	0 +1/2	3/5 −2/5	+3/2 +3/2
		0 −1/2	3/5 2/5
		−1 +1/2	2/5 −3/5

			5/2 3/2
			−3/2 −3/2
	−1 −1/2	4/5 1/5	5/2
	−2 +1/2	1/5 −4/5	−5/2
		−2 −1/2	1

3/2 × 1/2

	2	+2
+3/2 +1/2	1	2 1 / +1 +1

			2 1
+3/2 −1/2	1/4 3/4		2 1
+1/2 +1/2	3/4 −1/4		−0 −0
	+1/2 −1/2	1/2 1/2	2 1
	−1/2 +1/2	1/2 −1/2	−1 −1
		−1/2 −1/2	3/4 1/4
		−3/2 +1/2	1/4 −3/4

			2
			−2
		−3/2 −1/2	1

			5/2 3/2 1/2
+1/2 −1	3/10 8/15		1/6
−1/2 0	3/5 −1/15		−1/3
−3/2 +1	1/10 −2/5		1/2

			5/2 3/2
			−3/2 −3/2
	−1/2 −1	3/5 2/5	5/2
	−3/2 0	2/5 −3/5	−5/2
		−3/2 −1	1

$$d^2_{10} = \sqrt{\tfrac{1}{2}}\sqrt{\tfrac{1}{6}}\, d^1_{0-1}d^1_{11} + \sqrt{\tfrac{1}{2}}\sqrt{\tfrac{2}{3}}\, d^1_{00}d^1_{10} + \sqrt{\tfrac{1}{2}}\sqrt{\tfrac{1}{6}}\, d^1_{01}d^1_{1-1}$$

$$+\sqrt{\tfrac{1}{2}}\sqrt{\tfrac{1}{6}}\, d^1_{1-1}d^1_{01} + \sqrt{\tfrac{1}{2}}\sqrt{\tfrac{2}{3}}\, d^1_{10}d^1_{00} + \tfrac{1}{2}\, d^1_{11}d^1_{0-1}$$

$$= -\sqrt{\tfrac{3}{2}} \sin\beta \cos\beta$$

$$d^2_{11} = \tfrac{1}{2}\, d^1_{00}d^1_{11} + \tfrac{1}{2}\, d^1_{01}d^1_{10} + \tfrac{1}{2}\, d^1_{10}d^1_{01} + \tfrac{1}{2}\, d^1_{11}d^1_{00}$$

$$= \tfrac{1}{2}(2\cos\beta - 1)(\cos\beta + 1)$$

$$d^2_{1-1} = \tfrac{1}{2}\, d^1_{0-1}d^1_{10} + \tfrac{1}{2}\, d^1_{00}d^1_{1-1} + \tfrac{1}{2}\, d^1_{1-1}d^1_{00} + \tfrac{1}{2}\, d^1_{10}d^1_{0-1}$$

$$= -\tfrac{1}{2}(2\cos\beta + 1)(\cos\beta - 1)$$

$$d^2_{20} = \sqrt{\tfrac{1}{6}}\, d^1_{1-1}d^1_{11} + \sqrt{\tfrac{2}{3}}\, d^1_{10}d^1_{10} + \sqrt{\tfrac{1}{6}}\, d^1_{11}d^1_{1-1}$$

$$= \sqrt{\tfrac{3}{8}} \sin^2\beta$$

$$d^2_{21} = \sqrt{\tfrac{1}{2}}\, d^1_{10}d^1_{11} + \sqrt{\tfrac{1}{2}}\, d^1_{11}d^1_{10} = -\tfrac{1}{2} \sin\beta(1 + \cos\beta)$$

$$d^2_{2-1} = \sqrt{\tfrac{1}{2}}\, d^1_{1-1}d^1_{10} + \sqrt{\tfrac{1}{2}}\, d^1_{10}d^1_{1-1} = \tfrac{1}{2} \sin\beta(\cos\beta - 1)$$

$$d^2_{22} = d^1_{11}d^1_{11} = \cos^4 \tfrac{\beta}{2}$$

$$d^2_{2-2} = d^1_{1-1}d^1_{1-1} = \sin^4 \tfrac{\beta}{2} \quad .$$

From Eqs. (2) and (6) the complete rotation matrix for second-order tensor operators then becomes:

$$D^2_{Q'Q}(\alpha\beta\gamma)=\begin{bmatrix} e^{-2i\alpha}(\cos^4\frac{\beta}{2})e^{-2i\gamma} & -e^{-2i\alpha}\frac{(\sin\beta)}{2}(\cos\beta+1)e^{-i\gamma} \\ e^{-i\alpha}\frac{(\sin\beta)}{2}(\cos\beta+1)e^{-2i\gamma} & e^{-i\alpha}\frac{(2\cos\beta-1)}{2}(\cos\beta+1)e^{-i\gamma} \\ \sqrt{\frac{3}{8}}(\sin^2\beta)e^{-2i\gamma} & \sqrt{\frac{3}{2}}\sin\beta\cos\beta(e^{-i\gamma}) \\ -e^{i\alpha}\frac{(\sin\beta)}{2}(\cos\beta-1)e^{-2i\gamma} & -e^{i\alpha}\frac{(2\cos\beta+1)}{2}(\cos\beta-1)e^{-i\gamma} \\ e^{2i\alpha}(\sin^4\frac{\beta}{2})e^{-2i\gamma} & -e^{2i\alpha}\frac{(\sin\beta)}{2}(\cos\beta-1)e^{-i\gamma} \end{bmatrix}$$

$$\begin{bmatrix} e^{-2i\alpha}(\sqrt{\frac{3}{8}}\sin^2\beta) & e^{-2i\alpha}\frac{(\sin\beta)}{2}(\cos\beta-1)e^{i\gamma} & e^{-2i\alpha}(\sin^4\frac{\beta}{2})e^{2i\gamma} \\ -e^{-i\alpha}(\sqrt{\frac{3}{2}}\sin\beta\cos\beta) & -e^{-i\alpha}\frac{(2\cos\beta+1)}{2}(\cos\beta-1)e^{i\gamma} & e^{-i\alpha}\frac{(\sin\beta)}{2}(\cos\beta-1)e^{2i\gamma} \\ \frac{1}{2}(3\cos^2\beta-1) & -\sqrt{\frac{3}{2}}\sin\beta\cos\beta(e^{i\gamma}) & \sqrt{\frac{3}{8}}(\sin^2\beta)e^{2i\gamma} \\ e^{i\alpha}(\sqrt{\frac{3}{2}}\sin\beta\cos\beta) & e^{i\alpha}\frac{(2\cos\beta-1)}{2}(\cos\beta+1)e^{i\gamma} & -e^{i\alpha}\frac{(\sin\beta)}{2}(\cos\beta+1)e^{2i\gamma} \\ e^{2i\alpha}(\sqrt{\frac{3}{8}}\sin^2\beta) & e^{2i\alpha}\frac{(\sin\beta)}{2}(\cos\beta+1)e^{i\gamma} & e^{2i\alpha}(\cos^4\frac{\beta}{2})e^{2i\gamma} \end{bmatrix}$$

where the successive lines correspond to Q'=2, 1, 0, -1, -2, and the columns are arranged in the same order from left to right. Special cases of importance are:

$$d^K_{Q'Q}(0) = \delta_{Q'Q}$$

$$d^K_{Q'Q}(\pi) = (-1)^{K-Q'} \delta_{Q',-Q}$$

$$d^K_{Q'Q}(2\pi) = (-1)^{2K} \delta_{Q'Q} \quad .$$

Symmetry relations and explicit expressions for the reduced rotation matrices for K=0, 1, 2 are to be found in Satchler (Sa 60).

In practice, only rotations in the scattering plane about the y-axis are usually used ($\alpha=\gamma=0$). Designating the rotated second-rank moments by $\langle T^R_{KQ} \rangle$, we find from Eqs. (1) and (7):

$$\langle T^R_{20} \rangle = \langle T_{2-2} \rangle D^2_{-20} + \langle T_{2-1} \rangle D^2_{-10} + \langle T_{20} \rangle D^2_{00} + \langle T_{21} \rangle D^2_{10} + \langle T_{22} \rangle D^2_{20}$$

$$\langle T^R_{21} \rangle = \langle T_{2-2} \rangle D^2_{-21} + \langle T_{2-1} \rangle D^2_{-11} + \langle T_{20} \rangle D^2_{01} + \langle T_{21} \rangle D^2_{11} + \langle T_{22} \rangle D^2_{21}$$

$$\langle T^R_{22} \rangle = \langle T_{2-2} \rangle D^2_{-22} + \langle T_{2-1} \rangle D^2_{-12} + \langle T_{20} \rangle D^2_{02} + \langle T_{21} \rangle D^2_{12} + \langle T_{22} \rangle D^2_{22}.$$

Employing the conjugation property

$$\langle T_{KQ} \rangle = (-1)^Q \langle T_{K,-Q} \rangle^* \ ,$$

we obtain a single 3×3 matrix which is sufficient to describe general rotations of the second-rank moments about the y-axis:

---

*Denotes complex conjugate.

$$\begin{bmatrix} \langle T^R_{20} \rangle \\ \langle T^R_{21} \rangle \\ \langle T^R_{22} \rangle \end{bmatrix} = \begin{bmatrix} \frac{1}{2}(3\cos^2\beta - 1) & -\sqrt{6}\sin\beta\cos\beta & \sqrt{\frac{3}{2}}\sin^2\beta \\ \sqrt{\frac{3}{2}}\sin\beta\cos\beta & 2\cos^2\beta - 1 & -\sin\beta\cos\beta \\ \sqrt{\frac{3}{8}}\sin^2\beta & \sin\beta\cos\beta & \frac{1}{2}(1+\cos^2\beta) \end{bmatrix} \begin{bmatrix} \langle T_{20} \rangle \\ \langle T_{21} \rangle \\ \langle T_{22} \rangle \end{bmatrix}$$

REFERENCES

(Al 60) M. A. Al-Jeboori, M. S. Bokhari, A. Strzalkowski, and B. Hird, Proc. Phys. Soc. (London) 75, 875 (1960).

(Ar 65) J. F. Arvieux, R. Beurtey, A. Garin, T. Mikumo, A. Papineau, and J. Thirion, Physics Letters 16, 149 (1965).

(Ar 67) J. Arvieux, P. Darriulat, D. Garreta, A. Papineau, A. Tarrats, and J. Testoni, Nuclear Phys. A94, 663 (1967).

(Ba 56) J. Baldwin, O. Chamberlain, E. Segre, R. Tripp, C. Wiegand, and T. Ypsilantis, Phys. Rev. 103, 1502 (1956).

(Ba 65) S. Baker, G. C. Phillips, G. Roy, and G. K. Walters, Phys. Rev. Letters 15, 115 (1965).

(Be 63) R. Beurtey, R. Chaminade, A. Falcoz, M. Faure, R. Maillard, D. McDaniels, T. Mikumo, A. Papineau, L. Schecter, and J. Thirion, Compt. rend. 256, 922 (1963).

(Be 67) E. M. Bernstein, G. G. Ohlsen, V. S. Starkovich, and W. G. Simon, Phys. Rev. Letters 18, 966 (1967).

(Bi 59) L. C. Biedenharn, Nuclear Phys. 10, 620 (1959).

(Bl 51) R. J. Blin-Stoyle, Proc. Phys. Soc. (London) A65, 452 (1951).

(Bl 59) R. J. Blin-Stoyle and M. A. Grace, Handbuch der Physik, S. Flügge, Ed. (Springer-Verlag, Berlin, 1959), Vol. 42, p. 558.

(Br 63) R. I. Brown and W. Haeberli, Phys. Rev. 130, 1163 (1963).

(Br 66) L. Brown, H. A. Christ, and H. Rudin, Nuclear Phys. 79, 459 (1966).

(Bu 60) J. Button and R. Mermod, Phys. Rev. 118, 1333 (1960).

(Ch 54) O. Chamberlain, E. Segre, R. Tripp, C. Weigand, and T. Ypsilantis, Phys. Rev. 95, 1104 (1954).

(Da 52) R. H. Dalitz, Proc. Phys. Soc. (London) A65, 175 (1952).

(Da 67) S. E. Darden, Am. J. Phys. 35, 727 (1967).

(Do 68) D. C. Dodder, private communication.

(Ex 67) P. Extermann, Nuclear Phys. A95, 615 (1967).

(Fa 57) U. Fano, Revs. Modern Phys. 29, 74 (1957).

(Ha 63) W. Haeberli, Polarization of Neutrons in Fast Neutron Physics II (Interscience Publ., 1963).

(He 52) M. Huesinkveld and G. Freier, Phys. Rev. 85, 80 (1952).

(Ig 61) G. Igo, W. Lorenz, and U. Schmidt-Rohr, Phys. Rev. 124, 832 (1961).

(Ja 59) M. Jacob and G. C. Wick, Annals of Phys. 7, 404 (1959).

(Ja 61) B. A. Jacobsohn and R. M. Ryndin, Nuclear Phys. 24, 505 (1961).

(Ke 68) P. W. Keaton, private communication.

(La 55) W. Lakin, Phys. Rev. 98, 139 (1955).

(La 58) A. M. Lane and R. G. Thomas, Revs. Modern Phys. 30, 257 (1958).

(Lo 67) J. M. Lohr, private communication.

(Mc 65) L. C. McIntyre, Ph.D. Thesis, University of Wisconsin (1965).

(Mc 66) L. C. McIntyre, A. Trier, and W. Haeberli, in Proceedings of the International Symposium on Polarization Phenomena of Nucleons. 2nd, Karlsruhe, Proceedings, edited by P. Huber et al. (Birkhauser Verlag, Stuttgart, Germany, 1966), p. 504.

(Mc 67a) L. C. McIntyre and W. Haeberli, Nuclear Phys. A91, 369 (1967).

(Mc 67b) L. C. McIntyre and W. Haeberli, Nuclear Phys. A91, 382 (1967).

(Me 61) E. Merzbacher, Quantum Mechanics (John Wiley and Sons, New York, 1963).

(Ne 27) J. von-Neumann, Gottinger Nachr. 245 and 273 (1927).

(Ne 64) Yu. A. Nemilov and L. A. Pobedonostsev, Soviet Phys.-JETP 18, 76 (1964).

(Pl 68) G. R. Plattner, private communication.

(Po 61) L. G. Pondrom and J. W. Daughtry, Phys. Rev. 121, 1192 (1961).

(Ra 64) J. Raynal, Ph.D. Thesis, University of Paris (1964); CEA Report R2511.

(Ro 57) M. E. Rose, Elementary Theory of Angular Momentum (John Wiley and Sons, Inc., New York, 1957).

(Ro 65) L. Rosen, J. G. Beery, A. S. Goldhaber, and E. H. Auerbach, Ann. Phys. (N.Y.) 34, 96 (1965).

(Sa 58) G. R. Satchler, Nuclear Phys. 8, 65 (1958).

(Sa 60) G. R. Satchler, The Scattering and Polarization of Spin One Particles, Oak Ridge National Laboratory Report ORNL-2861 (1960).

(Sc 55) L. I. Schiff, Quantum Mechanics (McGraw-Hill, New York, 1955) 2nd edition.

(Sc 67) P. Schwandt and T. J. Yule, private communication.

(Sc 68) P. Schwandt, Nuclear Phys. A110, 585 (1968).

(Se 64a) F. Seiler, S. E. Darden, L. C. McIntyre, and W. G. Weitkamp, Nuclear Phys. 53, 65 (1964).

(Se 64b) L. S. Senhouse and T. A. Tombrello, Nuclear Phys. 57, 624 (1964).

(Sh 57) M. I. Shirokov, J. Exptr. Theoret. Phys. (U.S.S.R.) 32, 1022 (1957); translation: Soviet Phys.-JETP 5, 835 (1958).

(Si 53) A. Simon, Phys. Rev. 92, 1050 (1953).

(St 55) H. P. Stapp, The Theory and Interpretation of Polarization Phenomena in Nuclear Scattering, University of California Radiation Laboratory Report UCRL-3098 (1955).

(St 60) L. Stewart, J. E. Brolley, and L. Rosen, Phys. Rev. 119, 1649 (1960).

(Ta 65) M. Tanifuji, Phys. Rev. Letters 15, 113 (1965).

(Tr 67) A. Trier and W. Haeberli, Phys. Rev. Letters 18, 915 (1967).

(Wo 49) L. Wolfenstein, Phys. Rev. 75, 1664 (1949).

(Wo 52) L. Wolfenstein and J. Ashkin, Phys. Rev. 85, 947 (1952).

(Yo 65) P. G. Young, M. Ivanovich, and G. G. Ohlsen, Phys. Rev. Letters 14, 831 (1965).

(Yo 67) P. G. Young, G. G. Ohlsen, and M. Ivanovich, Nuclear Phys. A90, 41 (1967).